catalysts

MDPI

Article

Ni/MgO-Al_2O_3 Hydrotalcite-Derived Catalysts for Sustainable Iso-Butanol Generation from Methanol/Ethanol Blends

Joachim Pasel [1,*], Justus Hüging [1], Quoc Khanh Tran [1] and Ralf Peters [1,2]

[1] Institute of Energy and Climate Research, IET-4: Electrochemical Process Engineering, Forschungszentrum Jülich GmbH, 52425 Jülich, Germany
[2] Synthetic Fuel, Ruhr-Universität. 150, 44801 Bochum, Germany
* Correspondence: j.pasel@fz-juelich.de; Tel.: +49-2461-61-5140

Abstract

The catalytically supported upgrading of green ethanol and green methanol mixtures can produce higher alcohols, such as iso-butanol, in a sustainable manner. Iso-butanol can be used as a feedstock to defossilize the chemical and transportation sectors. MgO-Al_2O_3 hydrotalcite-based catalysts are a promising option for this purpose. In this paper, samples were synthesized using co-precipitation and urea methods with different Mg/Al molar ratios with Ni acting as the active catalytic component. Thereby, the catalysts synthesized using the urea method exhibited the greatest activity, producing iso-butanol concentrations of up to 170 mmol L^{-1} at 185 °C, with selectivities towards iso-butanol of 85–89% and a maximum space–time yield of 8.2 mmol g^{-1} h^{-1}. The most active catalyst among all samples from this paper was characterized by 100% proportions of strong basic and medium acidic catalyst sites and the largest specific surface area. XRD analysis revealed the presence of NiO, MgO and the spinels Al_2NiO_4 and Al_2MgO_4 in both synthesis variants as well as elemental Ni in one sample from the urea synthesis. CO_2-TPD and NH_3-TPD experiments showed the dominance of strong basic and medium/strong acidic catalyst sites in both synthesis pathways.

Keywords: mixed alcohols; catalytic upgrading; iso-butanol; Ni/MgO-Al_2O_3 hydrotalcite-derived catalysts; Guerbet reaction

1. Introduction

Using the diagram shown in Figure 1 for the so-called Guerbet reaction, iso-butanol can be produced from ethanol and methanol in a reaction mechanism that involves two successive methylation steps. In the first step, ethanol and methanol are first dehydrogenated to acetaldehyde and formaldehyde, which then react on a basic catalyst to acrolein in an aldol condensation step. Then, acrolein is hydrogenated to 1-propanol. In the second methylation step, 1-propanol reacts in very similar sequences to form iso-butanol. If ethanol and methanol were obtained from green H_2 and CO_2 separated from industrial waste gases or ambient air, the iso-butanol molecule synthesized can also be described as sustainable. Sustainable iso-butanol can contribute to the defossilisation of some CO_2-intensive areas: as a drop-in component to conventional fuels (gasoline, aviation and marine fuels), as a chemical precursor (butenes, butadiene, isobutyl acetate, pharmaceuticals and fragrances) and as an industrial solvent (paints, coatings, inks, adhesives) [1–11].

Check for updates

Received: 28 January 2026
Revised: 31 March 2026
Accepted: 2 April 2026
Published: 16 April 2026

Copyright: © 2026 by the authors. Licensee MDPI, Basel, Switzerland. This article is an open access article distributed under the terms and conditions of the Creative Commons Attribution (CC BY) license.

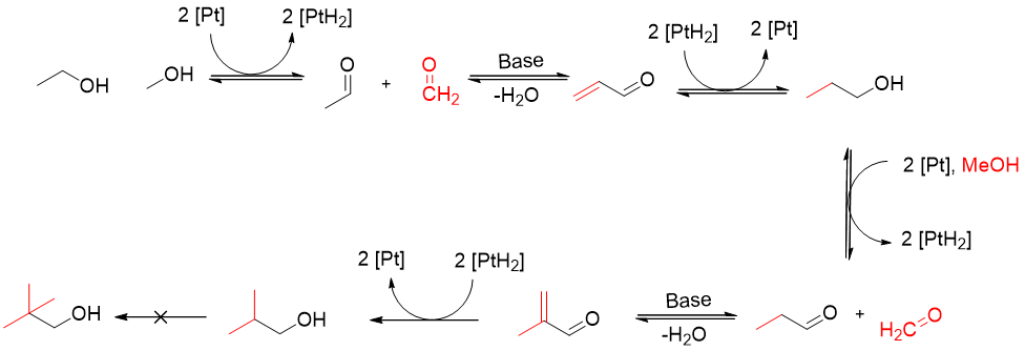

Figure 1. Reaction pathway for the synthesis of iso-butanol from ethanol and methanol [12].

Among the catalysts suitable for this reaction scheme, hydrotalcite-derived mixed oxides play a special role.

Hydrotalcites are minerals that belong to the class of layered materials. Their layers alternate between cationic sheet layers and anionic interlayers. Compared to regular clays, hydrotalcites have positively charged layers. The anionic interlayers compensate for the charge. The wide range of ions, which are applicable to each layers, enables a variety of possible compositions [13]. The applications of hydrotalcites range widely from catalysts over gas adsorbents to drug carriers [14]. In this paper, the focus will be on their properties as a catalyst support. For this purpose, they need to be converted into a mixed oxide by means of calcination. The water stored in the interlayers leaves between 150 °C and 200 °C. In the range of 300 °C to 600 °C, the interlayer anions decompose and leave as gases. At the same time, the octahedral brucite-like structure collapses, and the mixed oxides form. These structural changes result in new properties. The mixed oxides derived from hydrotalcites possess remarkable stability towards high temperatures. Furthermore, the specific surface area for the deposition of additional active catalytic sites increases significantly due to the removal of interlayer anions [15].

Li et al. [16] examined a series of Cu/NiAlOx catalysts based on a NiAl hydrotalcite precursor for the synthesis of iso-butanol from ethanol. At 250 °C, they observed a 35% conversion of ethanol with a selectivity for iso-butanol of 45%. Zhu et al. [17], on the other hand, investigated a Cu supported on MgAl layered hydrotalcite catalyst for the reaction of ethanol to butanol, which was not further calcined to the mixed oxides. The authors emphasize the importance of the interaction between Cu and LDH for catalytic activity. Bravo-Suárez et al. [18] synthesized Cu/MgAlOx mixed metal oxides for the coupling of ethanol and methanol. The highest activity for the C-C coupling reaction was found with a loading of 21 at% Cu. Using in situ FTIR, the authors identified formate and acetate as important intermediates. Wu et al. [19] investigated Ni/MgAlOx catalysts for the synthesis of biofuels from acetone/butanol/ethanol mixtures. Higher Mg/Al molar ratios led to strong basic sites on the catalyst surface and promoted the formation of long-chain hydrocarbons. Hydrotalcite-based MgAlOx and CuMgAlOx catalysts for the Guerbet reaction of methanol with methanol were investigated by Cheng et al. [20,21]. They found moderate basic sites and Cu^0 species to be particularly important, as together they promoted the condensation reaction between acetaldehyde and formaldehyde. Carlini et al. investigated the reaction between methanol and n-propanol at 200 °C on a catalyst consisting of two components: Cu-chromite and MgAl mixed oxides with different Mg/Al molar ratios. The mixed oxides were based on corresponding hydrotalcite precursors. The catalysts proved to be tolerant to the H_2O produced and showed no deactivation at selectivities close to 100% for iso-butanol. Lower Mg/Al molar ratios improved the catalytic activity, which the authors explain by a gain in medium-strength and strong basic centers on the catalyst surface [22]. In a subsequent paper, Carlini et al. doped the Mg-Al mixed

oxides with Cu, which allowed lower temperatures to be set with comparable catalytic activity [23]. Larina et al. [24] went one step further with their MgAl mixed oxides and investigated the Guerbet condensation between ethanol and 1-butanol to 2-ethyl-1-hexanol. They identified acid–base Lewis pairs at the interface between MgO and Al_2O_3 as crucial. At a Mg/Al molar ratio of 2, a maximum yield of 10.8% 2-ethyl-1-hexanol was found.

This brief literature review has clearly illustrated the importance of basic catalyst centers for the success of the aldol condensation between the aldehydes shown in Figure 1. Many other research groups have also emphasized the importance of Ni as an active component in dehydrogenation reactions, which are also of central importance in the conversion of methanol, ethanol and propanol to the corresponding aldehydes shown in Figure 1 [19,25–32]. The catalyst system investigated in this paper considers that both basicity and dehydrogenation activity are required to complete the reaction scheme shown in Figure 1. It therefore combines hydrotalcite-derived MgAl mixed oxides as a basic catalyst support having a high specific surface area with Ni as the active dehydrogenation component.

The overall approach of this paper is outlined below:

- To apply two different routes to the synthesis of Ni/Mg-Al mixed oxides catalysts. Many ways to synthesize hydrotalcites were already proposed in the past [33,34]. The methods chosen for this paper are co-precipitation and urea hydrolysis precipitation due to their simplicity. The approach utilizing urea hydrolysis is intended to result in homogeneous distribution of the precipitation agent. This homogeneity should result in a narrower particle size distribution and enhanced crystallinity.
- To investigate the influences of these syntheses' routes on the structural properties and the catalytic activity of the synthesized catalysts for the above-presented Guerbet reaction, yielding iso-butanol.
- To apply mild reaction conditions with a reaction temperature of 185 °C and a low pressure of 6 bar.

2. Results and Discussion

Regardless of the synthesis route, the mass fraction of Ni was always 10%, while the molar ratio of Mg/Al varied between 1:1 and 5:1 for both synthesis routes. For the sake of simplicity, a catalyst with 10 wt% Ni and, for example, a molar ratio of Mg/Al of 3:1 is abbreviated as 10Ni/Mg3Al1_coprec in the following text, while a sample prepared using the urea method with 10 wt% Ni and a molar ratio of Mg/Al of 3:1 is referred to as 10Ni/Mg3Al1_urea. 10 wt% Ni was chosen as the constant loading, as previous experiments by our group on the variation in the Ni mass fraction have shown that this value is optimal for catalytic activity [35].

2.1. Ni-Mg/Al Mixed Oxides Synthesized via the Co-Precipitation Method

In this section, the experimental results from catalyst characterization (temperature-programmed desorption, X-ray diffraction, inductively coupled plasma with optical emission spectroscopy, scanning electron microscopy, and N_2 sorption) with the five catalysts synthesized through the co-precipitation method are described and explained. In addition, the results of the catalytic tests are presented.

2.1.1. Temperature-Programmed Desorption (TPD) of CO_2 and NH_3

The temperature-programmed adsorption and desorption of specific gases, such as CO_2 and NH_3, enables the nature of the catalytic sites (basic or acidic, with different strengths) on the surface of a catalyst to be examined. The temperature range at which

desorption occurs determines the strength of the respective catalytic sites. Just as CO_2 is used to identify basic sites on a surface, NH_3 can reveal information about its acidic centers.

Figure 2 shows the TPD profiles of the five catalysts prepared via the co-precipitation method. The CO_2 desorption profiles are shown on the left, and the NH_3 desorption profiles are shown on the right. Choudhary and Rane investigated the relationship between the desorption temperature and strength of the catalytic site and concluded that the desorption occurs in multiple steps [36]. The first desorption step takes place between 50 °C and 150 °C, indicating weak basic sites. Subsequently, the temperature range from 150 °C to 300 °C corresponds to basic sites with medium strength. The strong and very strong basic sites are observed in the temperature ranges from 300 °C to 500 °C and 500 °C to 900 °C, respectively [36].

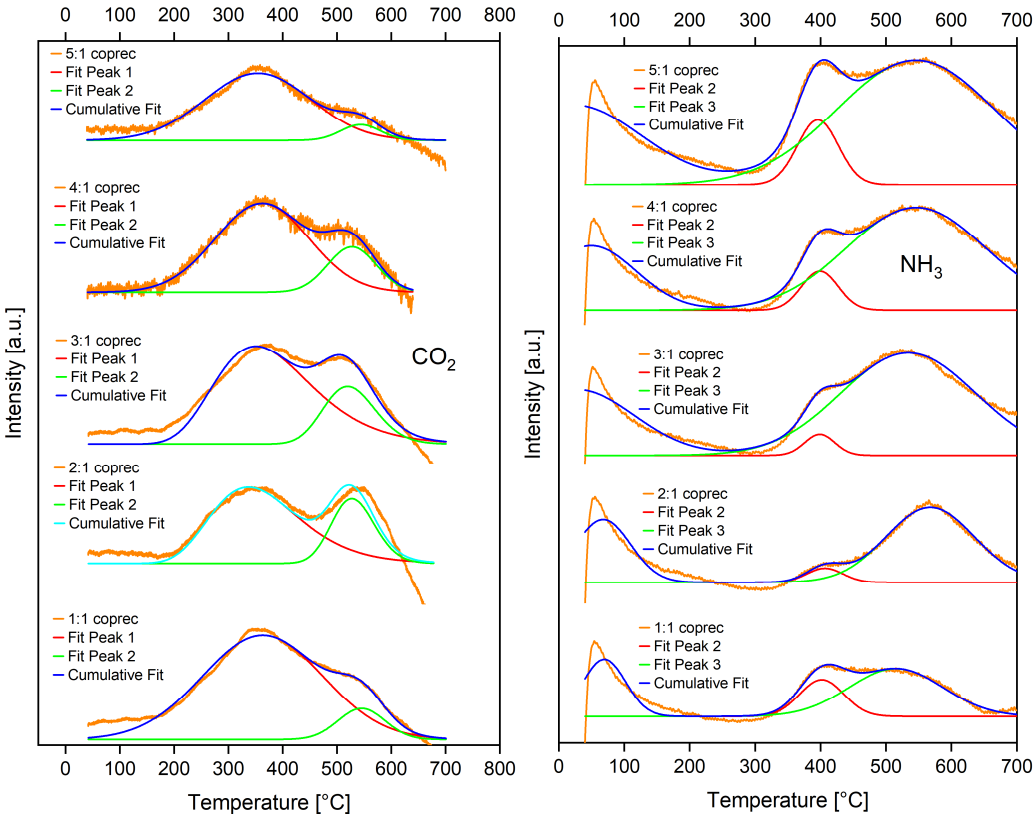

Figure 2. TPD profiles ((**left**) CO_2, (**right**) NH_3) of the five catalysts prepared via the co-precipitation method.

In Figure 2, it becomes obvious that the CO_2-TPD profiles of the five catalysts from the co-precipitation method were similar. They showed a broad peak between approximately 200 °C and 650 °C with a shoulder in the temperature range between approximately 450 °C and 620 °C. This shoulder was particularly pronounced in the case of the catalyst with a Mg/Al molar ratio of 2:1. The profiles show that strong and very strong basic centers dominated on these catalysts. This property may have a positive impact on the activity for the synthesis of iso-butanol, as this reaction proceeds via an aldol condensation pathway as explained in Figure 1, which involves the abstraction of an H-atom from the β-carbon atom in acetaldehyde, for which strong basicity is required. In the first two columns, Table 1 shows the percentages of strong and very strong basic sites on the five catalysts from the co-precipitation method calculated from these profiles. The strong basic centers predominated over the very strong basic sites for each of these samples. Except for the sample with a Mg/Al molar ratio of 1:1, there is a correlation between the Mg/Al molar ratio and the

proportion of strong basic sites on the catalyst surface. This increased continuously with rising Mg/Al molar ratio and reached 92% in the case of the 10Ni/Mg5Al1_coprec catalyst.

Table 1. Percentage distribution of basic (from CO_2-TPD) and acidic (from NH_3-TPD) centers of different strengths on the five catalysts synthesized via the co-precipitation method.

Catalysts	Strong Basic [%]	Very Strong Basic [%]	Weak Acidic [%]	Medium Acidic [%]	Strong Acidic [%]
10Ni/Mg1Al1_coprec	89.5	10.5	28.5	19.0	52.5
10Ni/Mg2Al1_coprec	65.8	34.2	32.5	4.8	62.7
10Ni/Mg3Al1_coprec	76.5	23.5	28.2	1.7	70.1
10Ni/Mg4Al1_coprec	78.9	21.1	26.9	6.7	66.4
10Ni/Mg5Al1_coprec	92.1	7.9	33.2	7.9	58.9

The strengths of the acidic sites are divided into weak, medium and strong ones [37]. Weak sites are observed up to a temperature of 250 °C, while medium sites appear from 250 °C to 450 °C. Desorption temperatures higher than those are associated with strong acidic sites. On the right side of Figure 2—as was observed in the case of CO_2-TPD—also the NH_3-TPD profiles of the five catalysts from the co-precipitation method were similar. They all showed a peak in the temperature range between approximately 50 °C and 200 °C as well as broad signals between 300 °C and 650 °C. In addition, Table 1 shows the percentages of weak, medium and strong acidic sites on these five catalysts in columns three to five. The strongly acidic catalyst centers dominated in all cases. The values were between approximately 53% and 70% with no clear dependence on the molar Mg/Al molar ratio being found. The percentages of weak acidic centers were between 27% and 33%. Here, again, no clear dependence on the molar Mg/Al molar ratio could be determined.

2.1.2. X-Ray Diffraction Analysis (XRD)

To gain insight into the morphologies of the five MgAl supports and the five Ni containing catalysts from the co-precipitation route in terms of composition, crystallinity, and crystal size, their XRD patterns were recorded with Cu Ka-radiation (λ = 1.54060 Å) and are presented in Figure 3 (MgAl supports) and Figure 4 (Ni-containing catalysts).

Figure 3 shows that all catalyst supports exhibited a predominantly amorphous character regardless of the Mg/Al molar ratio. At 2Θ values of 11.5° and 23.1°, reflections were observed in the cases of the Mg3Al1_coprec and Mg1Al1_coprec supports, which can be attributed to the free lattice oxygen phases that formed during the synthesis of the supports. The diffractograms of all five MgAl supports shared distinct signals at approximately 43.3° (separate phases of periclase MgO (COD 9000500) [38] and corundum Al_2O_3 (COD 9008081) [38]) and 62.5° (periclase MgO (COD 9000500) [38]). Furthermore, all five diffractograms exhibited shoulders, some of which were very weak, at approximately 35.0° and 79.2°. The reflections at 35.0° could be attributed to Al_2O_3 (COD 9008081) [38], and those at 79.2° could be attributed to two separate phases of MgO (COD 9000500) [38] and the spinel phase Al_2MgO_4 (COD 9002852) [38]. Except for the catalyst support Mg3Al1_coprec, a significant increase in the intensities of the signals at 43.3° and 62.5° was observed for the other four supports as the Mg/Al molar ratio increased. This trend could be attributed to an increase in the crystallinity and/or the crystallite size of the respective phases.

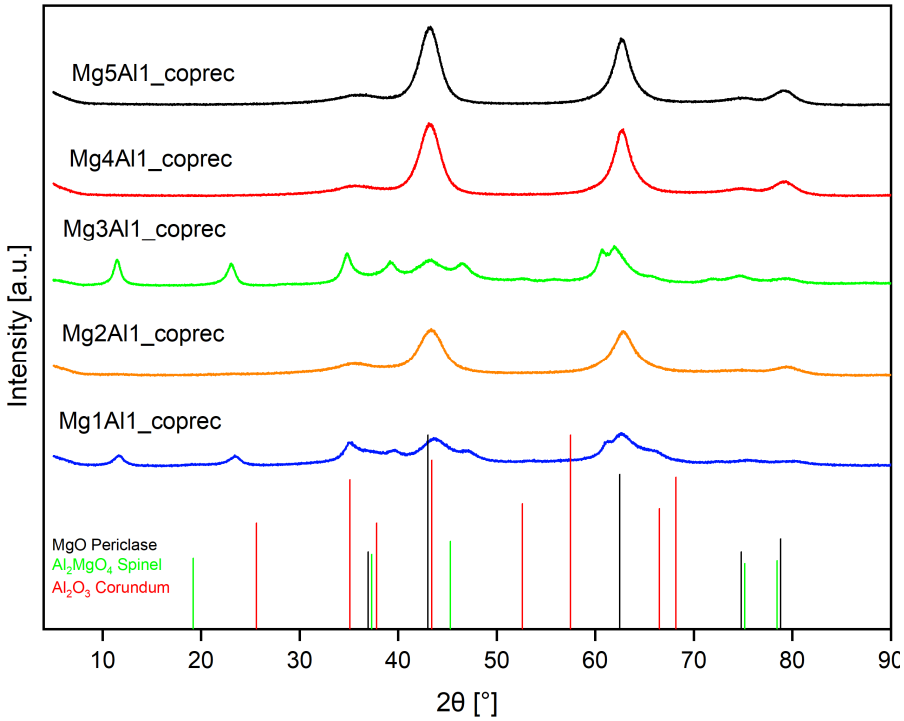

Figure 3. XRD patterns of the five MgAl supports prepared via the co-precipitation method.

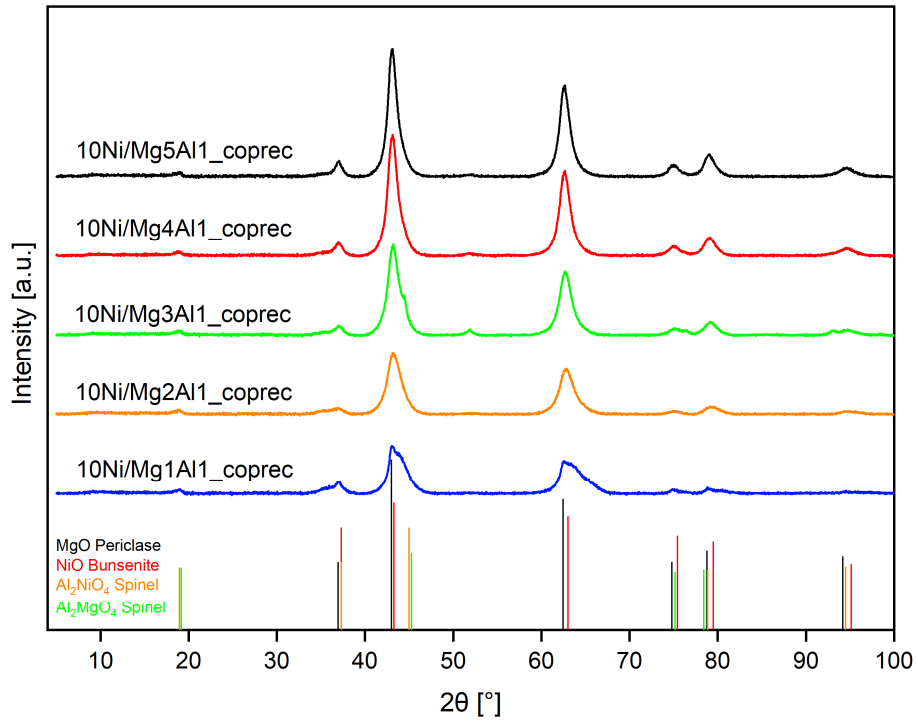

Figure 4. XRD patterns of the five Ni containing catalysts prepared via the co-precipitation method.

It becomes evident from Figure 4 that for the Ni-containing catalysts from the co-precipitation route, the most dominant peaks for all spectra could be observed at approximately 43.0° and 62.5°, respectively. These peaks were attributed to MgO in a periclase phase (COD 9000500) [38] and NiO in a bunsenite phase (COD 9008693) [38], respectively. There were further smaller reflections at approximately 37.0°, 74.9°, 79.9°, and 94.7°, whose intensities were at least partly due to MgO and NiO. In addition, a weak signal at approximately 18.8° was observed for all spectra, which could be solely attributed to the Al_2NiO_4 and Al_2MgO_4 spinel phases (COD 9001442 and 9002852) [38]. A phase for elemental Ni

could not be found in any of the five XRD patterns. Evidently, the Ni sites oxidized to NiO during the period between the final reduction step of impregnation with Ni (see Section 3.1.3) and the execution of the XRD experiments. When the XRD patterns of the five catalysts are compared with each other, it is noticeable that the intensities of the dominant peaks at 43.0° and 62.5°, respectively, increased significantly as the molar ratio of Mg/Al increased. Since the amount of Ni on the support surface was constantly set to 10 wt% the described increase in the intensities could be attributed to an increase in the crystallinity and/or the crystallite size of MgO. The intensities of the reflection solely belonging to the spinel phases Al_2NiO_4 and Al_2MgO_4 at 18.8° did not significantly change as the molar ratio of Mg/Al increased. That would mean that the crystallinity and/or the crystallite size of the two spinel phases did not change when the Mg/Al molar ratio increased. Figure 5 illustrates the crystallite size for the dominant MgO phase and the spinel phase calculated via the Scherrer equation.

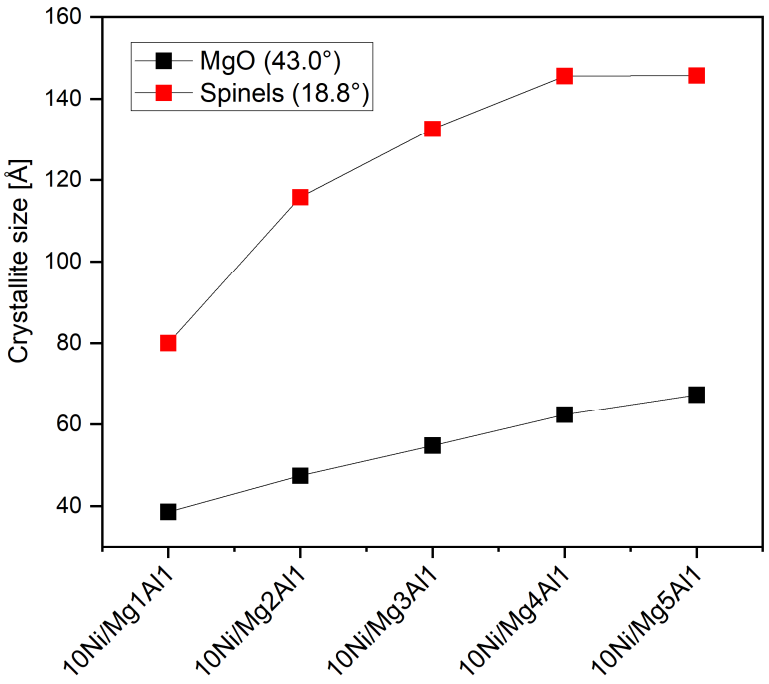

Figure 5. Crystallite sizes of the five Ni-containing catalysts prepared via the co-precipitation method.

In both cases, the crystallites grew with increasing molar ratio of Mg/Al. In the case of the spinel phases, a strong increase from approximately 80 Å to 145 Å was observed, while the crystallite size of the MgO phase increased much less strongly from 39 Å to 67 Å. The findings from Figure 5 contradict the conclusion from Figure 4 that the spinel phases remained unchanged as the molar fraction of MgO increased. Their crystallite size even increased by a greater amount than those of MgO. Clearly, the intensities of the reflections for the spinel phases in Figure 4 were too low to allow a clearly visible increase to be detected. Therefore, the XRD result is that a higher Mg/Al molar ratio led to higher crystallinity and larger crystallites in the MgO and spinel phases. All experimental data for Figure 5 are summarized in Table S1 in the Supplementary Information.

2.1.3. Inductively Coupled Plasma with Optical Emission Spectroscopy (ICP-OES)

Table 2 compares the Ni mass fractions and the Mg/Al molar ratios of the five catalysts from the co-precipitation method, as determined via ICP–OES measurements and calculated based on experimental quantities, respectively. As presented in the table, the actual quantities of Ni after impregnation only differed slightly from the calculated values.

The greatest deviation occurred at the 2:1 ratio, while the measured value at the 5:1 ratio was closest to the calculated value. This analysis demonstrates that impregnation via rotary evaporation was effective. However, greater deviations were observed with respect to the Mg/Al molar ratio. The calculated values closely matched the desired ratios from 1:1 to 5:1, whereas the ICP-OES values differed significantly from the calculated/desired numbers for ratios greater than 3:1. Therefore, it can be concluded that as the molar Mg/Al molar ratio increased, less Mg precipitated alongside Al to form the hydrotalcite structure. One reason for this difference may be that the pH value of 10 set during synthesis was too low to precipitate the Mg ions quantitatively as $Mg(OH)_2$, whereas this was already the case for the Al ions (as $Al(OH)_3$) at this pH value.

Table 2. Comparison of the Ni mass fractions and the molar ratios of Mg/Al (co-precipitation method) determined via: (i) ICP–OES measurements and (ii) ciphered based on experimental quantities.

Catalysts	Ni Mass Fraction [wt%]		Molar Ratios of Mg/Al [–]	
	ICP-OES	Calculated	ICP-OES	Calculated
10Ni/Mg1Al1_coprec	9.20 ± 0.30	11.26	0.95:1	0.98:1
10Ni/Mg2Al1_coprec	8.66 ± 0.11	11.15	1.97:1	2.00:1
10Ni/Mg3Al1_coprec	8.85 ± 0.07	11.17	2.64:1	3.01:1
10Ni/Mg4Al1_coprec	9.19 ± 0.05	11.48	3.03:1	4.00:1
10Ni/Mg5Al1_coprec	9.76 ± 0.08	11.14	3.29:1	5.00:1

2.1.4. Scanning Electron Microscopy (SEM)

Figure 6 shows an SEM image of the Mg1Al1_coprec support at a magnification of 1000 (top left), an SEM image of the catalyst Ni/Mg1Al1_coprec at a magnification of 10,000 (top right), and EDX element mappings (bottom), which belong to the image at the top right.

A large structure measuring a few hundred micrometers with smaller particles distributed across its surface was observed on the top left. The particles seemed to be distributed evenly across the surface of the larger structure and ranged in size from around 1 µm to 20 µm. They varied in shape, ranging from cubes to shards and asymmetric structures. The image on the right provides a closer look at the surface of the larger structure as well as a detailed close-up of the smaller particles. This image reveals that the surface was more uneven than suggested by the first image. The smaller particles consisted of layered clusters ranging in size from nanometers to micrometers.

The large structure was most likely an Al_2MgO_4 spinel formed during the precipitation process. As not all Mg ions were incorporated into the hydrotalcite structure during synthesis, the remaining ions precipitated as $Mg(OH)_2$, which was then converted into MgO during calcination. Based on the EDX mappings in the bottom of this figure, it can be concluded that this MgO represented most of the small particles on top of the Al_2MgO_4 spinel. A detailed size analysis reveals that almost all particles on the surface had an area smaller than 20 μm^2. Most particles showed an area of up to 1 μm^2. The EDX mapping for Ni in the Ni/Mg1Al1_coprec catalyst reveals that Ni was uniformly distributed over the surface of the MgAl support.

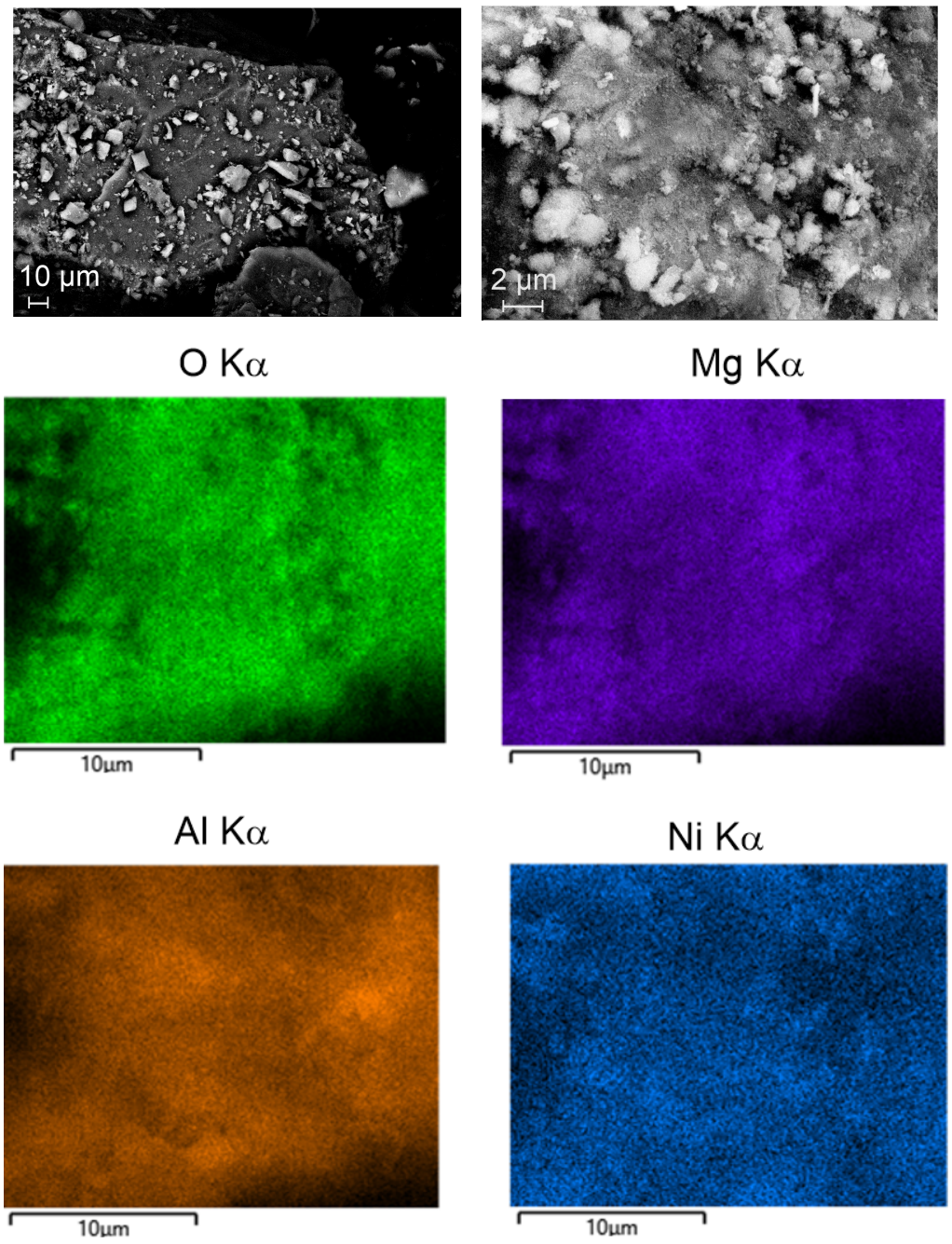

Figure 6. SEM image of the Mg1Al1_coprec support at a magnification of 1000 (**top left**), SEM image of the catalyst Ni/Mg1Al1_coprec at a magnification of 10,000 (**top right**), and EDX element mappings (**bottom**), which belong to the image at the top right.

2.1.5. N_2 Sorption

Table 3 displays the results of the N_2 sorption measurements with the five Ni-doped catalysts synthesized via the co-precipitation method and with the respective MgAl supports. The Ni-doped catalyst with a Mg/Al molar ratio of 1:1 had the highest values for the surface area, the pore volume and the average pore size. Beyond this, there were no clear trends. Only in the case of the average pore size was there a tendency for its values to decrease as the Mg/Al molar ratio increased. When comparing the results for the surface area, the pore volume and the average pore size of the Ni-containing catalysts with their respective supports at the same Mg/Al molar ratio, it is noticeable that the undoped supports consistently exhibited higher numerical values. For example, the support Mg1Al1_coprec

had a higher surface area value of 278.8 m^2 g^{-1} than the catalyst 10Ni/Mg1Al1_coprec with 253.6 m^2 g^{-1}. Another example is the pore volume of the 10Ni/Mg5Al1_coprec catalyst, which at 0.47 cm^3 g^{-1} was smaller than that of the corresponding Mg5Al1_coprec support at 0.60 cm^3 g^{-1}. In each case, doping with Ni led to a reduction in surface area and a narrowing of the pore system.

Table 3. Results of the N_2 sorption measurements with the five catalysts synthesized via the co-precipitation method and with the respective supports.

Catalysts	Surface Area [m^2 g^{-1}]	Pore Volume [cm^3 g^{-1}]	Average Pore Size [Å]
Mg1Al1_coprec	278.8	0.78	60.4
Mg2Al1_coprec	240.6	0.62	58.2
Mg3Al1_coprec	230.7	0.59	55.1
Mg4Al1_coprec	272.5	0.71	54.5
Mg5Al1_coprec	291.3	0.60	51.2
10Ni/Mg1Al1_coprec	253.6	0.73	57.7
10Ni/Mg2Al1_coprec	114.6	0.30	52.7
10Ni/Mg3Al1_coprec	128.2	0.34	53.2
10Ni/Mg4Al1_coprec	227.4	0.61	53.2
10Ni/Mg5Al1_coprec	208.3	0.47	44.7

2.1.6. Catalytic Activity

Figure 7 shows the results of the catalytic tests with respect to the synthesis of iso-butanol at a reaction temperature of 185 °C with the five catalysts prepared via the co-precipitation method. Blank experiments without catalyst but with all other components of the reactant mixture, including NaOH, showed no catalytic activity. For the representation of this figure, the actual values for the catalyst compositions from Table 2 were chosen. Based on the reduction step at 550 °C described in Section 3.1.3 with the calcined NiO/MgO-Al_2O_3 samples, it can be assumed that elemental Ni was present as the catalytically active center for the dehydrogenation and hydrogenation steps in the scheme from Figure 1 in all catalytic experiments. The high proportions of strong basic and strong acidic catalyst centers shown in Figure 2 and Table 1 can be assigned the function of being responsible for the aldol condensation (strong basic) and C-C coupling (strong acidic) steps in this scheme. The figure on the top left regarding the concentration of iso-butanol as a function of reaction time illustrates a clear dependence of the concentration of iso-butanol on the Mg/Al molar ratio of the respective catalysts. The higher the Mg/Al molar ratio, the higher the iso-butanol concentrations. With samples 10Ni/Mg3.03Al1 and 10Ni/Mg3.29Al1, values for the concentration of iso-butanol between 135 mmol L^{-1} and 140 mmol L^{-1} were achieved in the reaction time range between 180 min and 240 min. From the finding that the trends shown flattened slightly with increasing reaction time, it can be concluded that the catalysts began to deactivate in this time range. Reasons for the possible deactivation of the catalysts may lie in carbonaceous deposits on the catalytically active sites that have formed during the reaction or in the irreversible adsorption of CO on these catalytically active centers. A similar picture can be seen in this figure on the top right when discussing the conversion of ethanol as a function of reaction time at different Mg/Al molar ratios. Again, samples 10Ni/Mg3.03Al1 and 10Ni/Mg3.29Al1 were the most active and reached conversions of almost 12% after a reaction time of 240 min. As discussed in Figure 2, the proportion of strong basic sites on the catalyst surface increased continuously as the Mg/Al molar ratio increased. From this, it can be deduced that there is also a direct correlation between catalytic activity and the proportion of strong basic sites on the catalyst surface. The greater this proportion, the more active the catalysts were for the synthesis of iso-butanol from

ethanol/methanol mixtures. Furthermore, a correlation between the crystallite sizes of MgO, which increased from approximately 4 nm in the 10Ni/Mg1Al1_coprec catalyst to approximately 7 nm in the 10Ni/Mg5Al1_coprec sample (see Figure 5), and the catalytic activity can be deduced. Slightly larger MgO crystallites led to better catalytic activities.

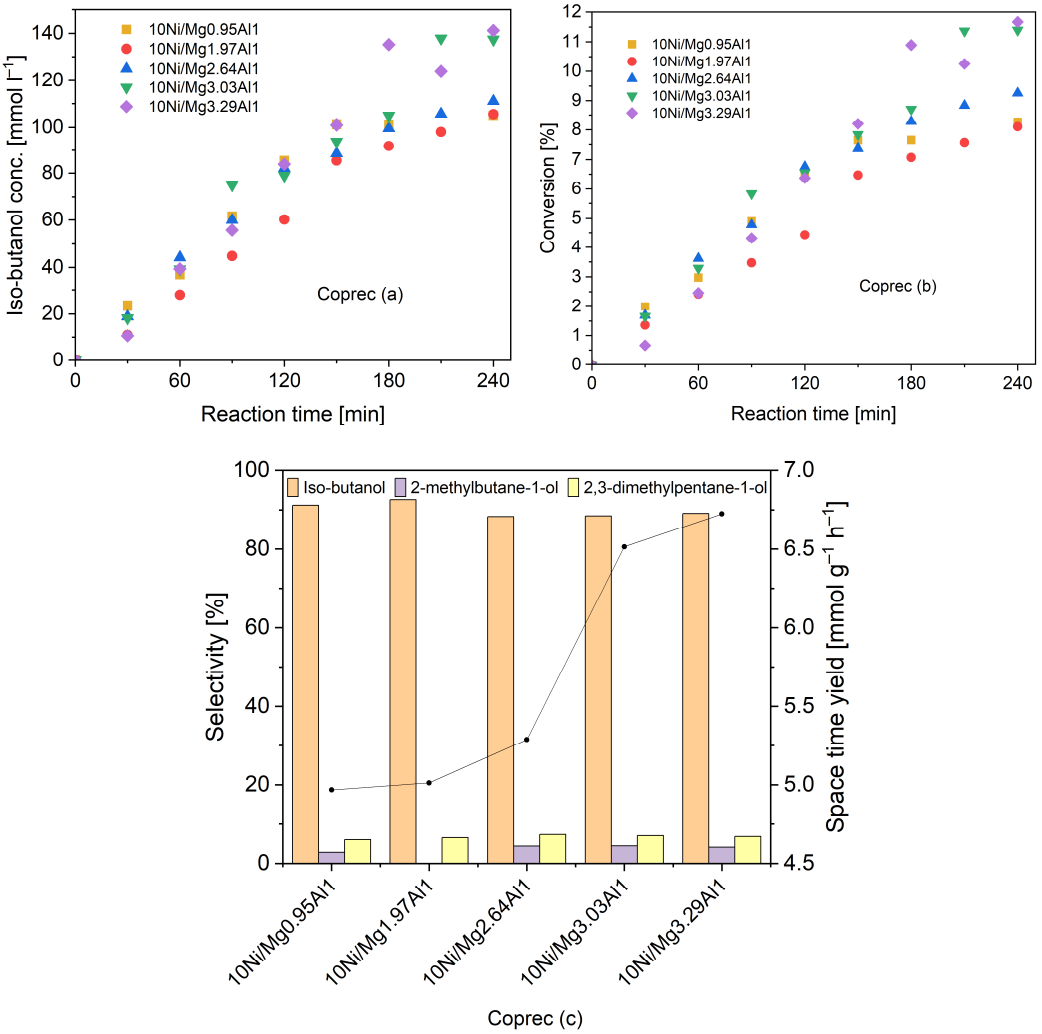

Figure 7. Results of the catalytic tests at a reaction temperature of 185 °C with respect to the synthesis of iso-butanol with the five catalysts prepared via the co-precipitation method, m(catalyst) = 250 mg, d(powder) < 75 µm, V(reactor) = 70 mL, c_0(EtOH) = 1600 mmol L^{-1}, c(NaOH) = 450 mmol L^{-1}, c(n-decane) = 15 mmol L^{-1}, methanolic solution. (**a**) Concentration of iso-butanol. (**b**) Ethanol conversion. (**c**) Selectivities towards iso-butanol and other main by-products (left), space–time yield at 240 min reaction time (right).

In the lower section of Figure 7, the selectivities of the individual catalysts towards the products iso-butanol, 2-methylbutane-1-ol and 2,3-dimethylpentane-1-ol are plotted on the left *Y*-axis. The reaction time was 240 min. The figure shows that the selectivity to iso-butanol was between 88% and 93% for all catalysts. A dependence on the Mg/Al molar ratio could not be found. Selectivity towards 2,3-dimethylpentane-1-ol was in the range of 6–7%, while that toward 2-methylbutane-1-ol was in the range of 0–4%. The space–time yield for the formation of iso-butanol of the catalysts, which is calculated according to Equation (1) from the molar quantity of iso-butanol formed, the catalyst mass and the reaction time, is shown in this figure on the right *Y*-axis. It was highest for the two samples 10Ni/Mg4Al1 and 10Ni/Mg5Al1 with values of 6.5 mmol g^{-1} h^{-1} and 6.7 mmol h^{-1} g^{-1},

respectively. All experimental data for Figure 7 are summarized in Tables S2 and S3 in the Supplementary Information.

$$STY = \frac{n(iso-butanol)}{m(catalyst) \times t(reaction)} \quad (1)$$

2.2. Ni-Mg/Al Mixed Oxides Synthesized via the Urea Method

In this section, the experimental results from catalyst characterization (temperature-programmed desorption, X-ray diffraction, inductively coupled plasma with optical emission spectroscopy, scanning electron microscopy, and N_2 sorption) with the five catalysts synthesized through the urea method are described and explained. In addition, the results of the catalytic tests are presented.

2.2.1. Temperature-Programmed Desorption (TPD) of CO_2 and NH_3

Figure 8 shows the TPD profiles of the five catalysts prepared via the urea method. The CO_2 desorption profiles are shown on the left and the NH_3 desorption profiles are shown on the right. All five samples in the left-hand figure showed a broad desorption peak for CO_2 in the temperature range between 300 °C and 500 °C, which suggests that strong basic centers dominated on the surfaces of these samples. Their percentage proportions ranged between 76% and 100% (see Table 4). Apart from sample 10Ni/Mg4Al1_urea, the slopes of the right flanks of the peaks were very low, which indicates a second peak. This peak was also quantitatively evaluable and can be attributed to very strong basic centers with percentage proportions ranging between 0% and 25% (see Table 4). This result is like that found with the samples produced by co-precipitation. There, too, the strong basic sites dominated. Strong or very strong basicity is a prerequisite for high catalytic activity in the Guerbet reaction. The NH_3 desorption profiles of the five urea method samples on the right in Figure 8 were very similar to each other except for the Mg/Al molar ratio of 4:1. Peaks were evident in the temperature range between approximately 50 °C and 200 °C, and there were also broad signals between 300 °C and 650 °C. Table 4 shows the percentages of weak, medium, and strong acidic sites on these four catalysts in columns three to five, which were calculated based on the measured profiles in Figure 8. As the Mg/Al molar ratio increased, a small increase in the fraction of weak and medium acidic sites was observed, while the fraction of strong acidic sites decreased. An increase in the Mg/Al molar ratio reduced the quantity of strong acidic sites in favor of an increase in weak and medium centers. In contrast, the profile of the 10Ni/Mg4Al1_urea catalyst differed significantly. Only one sharp signal, with a peak at 410 °C, was observed. Rather than possessing all three types of acid strength, sample 10Ni/Mg4Al1_urea exclusively exhibited medium acidic sites (see Figure 8).

2.2.2. XRD Analysis

To analyze the five urea-route MgAl supports and the five Ni-containing catalysts concerning composition, crystallinity, and crystal size, their XRD patterns were recorded using Cu Kα-radiation (λ = 1.54060 Å) and are presented in Figure 9 (MgAl supports) and Figure 10 (Ni-containing catalysts).

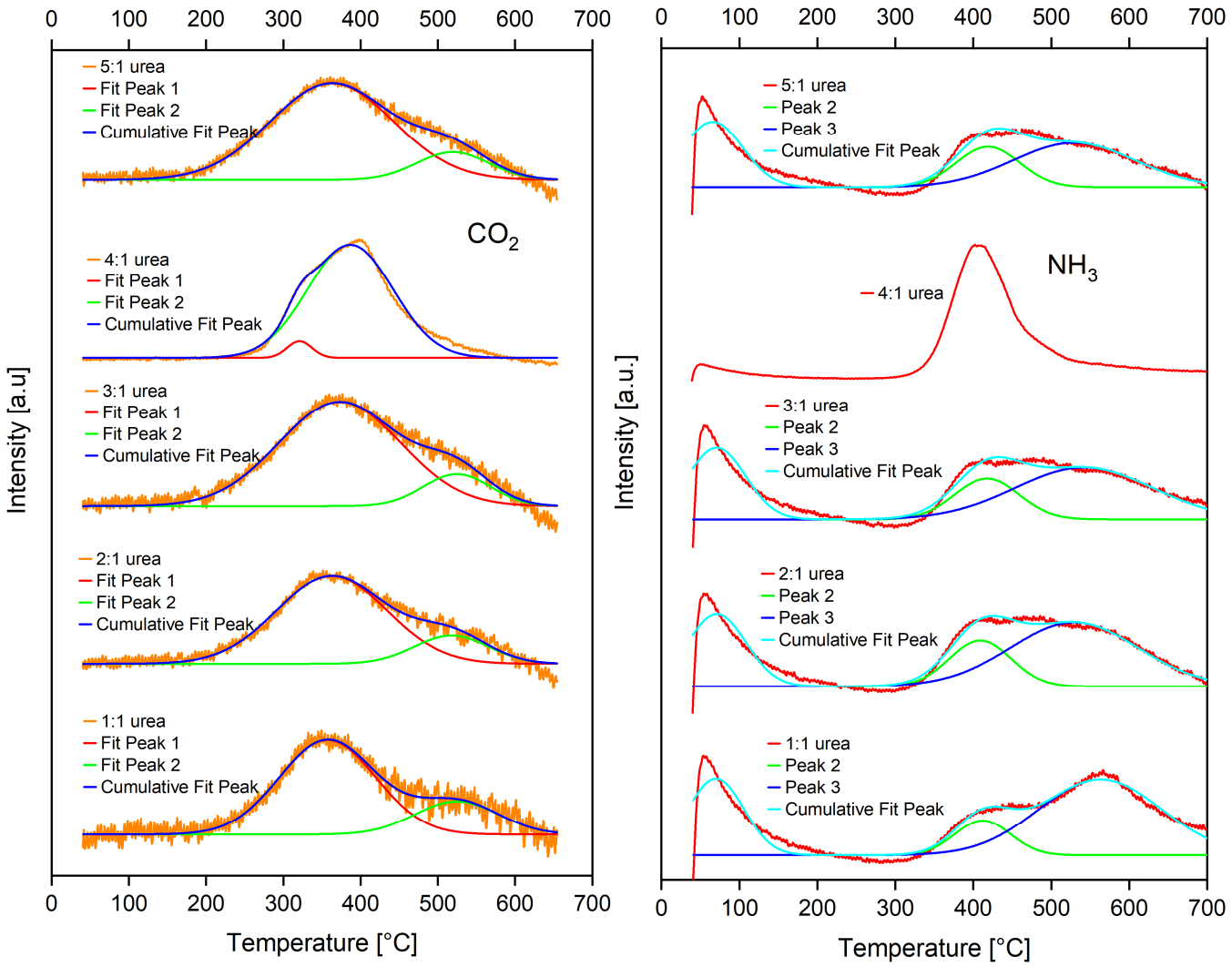

Figure 8. TPD profiles ((**left**) CO_2, (**right**) NH_3) of the five catalysts prepared via the urea method.

Table 4. Percentage distribution of basic (from CO_2-TPD) and acidic (from NH_3-TPD) centers of different strengths on the five catalysts synthesized via the urea method.

Catalysts	Strong Basic [%]	Very Strong Basic [%]	Weak Acidic [%]	Medium Acidic [%]	Strong Acidic [%]
10Ni/Mg1Al1_urea	76.1	24.9	27.6	12.4	60.0
10Ni/Mg2Al1_urea	82.2	17.8	27.8	18.6	53.6
10Ni/Mg3Al1_urea	85.4	14.6	29.7	19.0	51.3
10Ni/Mg4Al1_urea	100.0	0.0	0.0	100	0.0
10Ni/Mg5Al1_urea	85.6	14.4	33.0	21.5	45.5

Like the MgAl supports produced using the co-precipitation method from Figure 3, the MgAl supports from the urea method also exhibited a predominantly amorphous character. Figure 9 shows two signals at 43.3° and 62.5° for all five samples. The signal at 43.3° can, similarly to the samples from the co-precipitation route, be attributed to separate phases of MgO in the periclase phase (COD 9000500) and Al_2O_3 in the corundum phase (COD 9008081) [38]. The reflection at 62.5° can be attributed to MgO in the periclase phase (COD 9000500) [38].

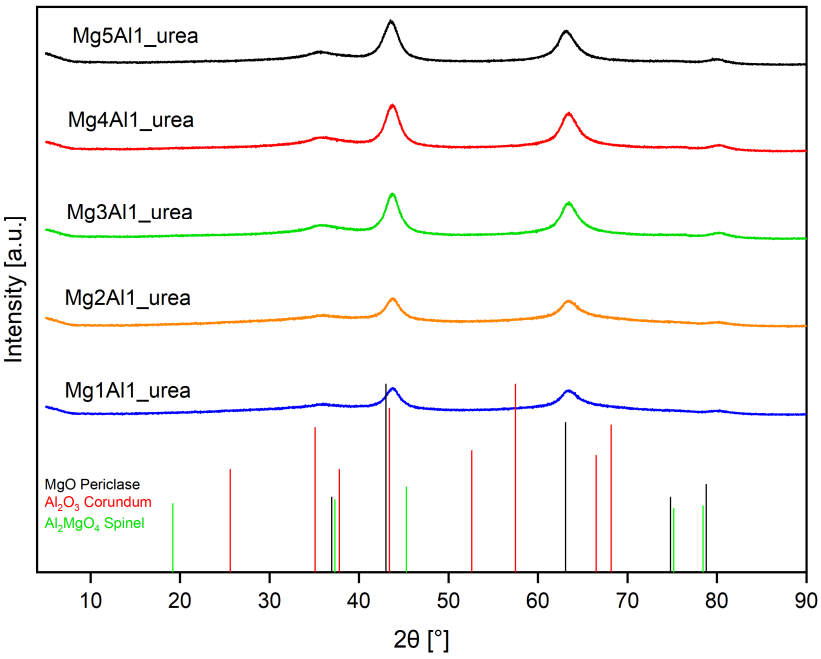

Figure 9. XRD patterns of the five MgAl supports prepared via the urea method.

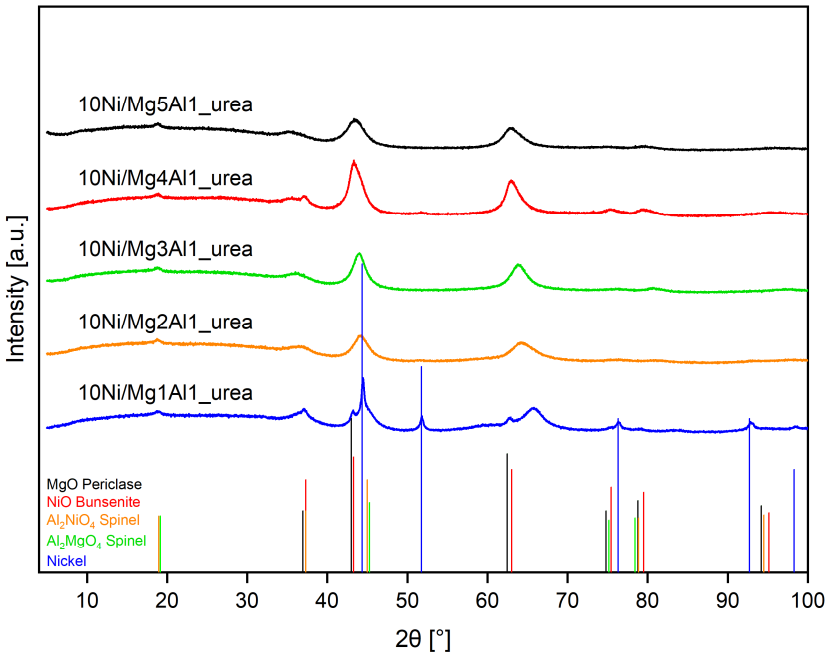

Figure 10. XRD patterns of the five Ni-containing catalysts prepared via the urea method.

In the case of the Ni-containing catalysts from the urea method, all five Mg/Al molar ratios exhibited characteristic peaks at around 43.0° and 62.4°, which are indicative of the reflections of MgO in the periclase phase (COD 9000500) [38] and NiO in the bunsenite phase (COD 9008693) [38]. Additionally, the small peaks at around 18.8° corresponded to the spinel phases Al_2NiO_4 and Al_2MgO_4 (COD 9001442 and 9002852) [38]. The group of peaks at 37.0° belonged to reflections of different phases, such as Al_2NiO_4, MgO and NiO. Notably, the pure Ni phase was visible in the sharp peaks at 44.4° and 51.6°, as well as in the group of peaks at approximately 76.2° and 92.8° for the 1:1 Mg/Al molar ratio (COD 9012970) [38], whereas no other ratio showed peaks belonging to pure Ni. The Ni component of this catalyst did not fully re-oxidize following reduction. For all other ratios, the Ni phase was well dispersed, amorphous, or had already been re-oxidized. For the

first four Mg/Al molar ratios (1:1 to 4:1), the reflections for the phases at 43.0° and 62.4° increased in peak height and area as the Mg/Al molar ratio increased. This indicates an increase in the amount of MgO, since the quantity of Ni was kept constant during synthesis. However, this trend did not continue for the 5:1 Mg/Al molar ratio. At the same time, the peak for the spinel phases at 18.8° remained constant in terms of height and area. As can be seen in Figure 11, the crystallite size of the MgO phases did not change significantly across the five ratios. The lack of value for the MgO phase at a Mg/Al molar ratio of 1:1 is due to the shape of the peak at 43.0°. The position of the elemental Ni reflex at 44.4° interferes with the MgO phase, meaning that no distinct peak could be isolated. Therefore, calculation of the crystallite size was not possible. The size of the spinel crystallites at 18.8° changed irregularly, ranging from a minimum of 85.5 Å to a maximum of 153.8 Å for the Mg/Al molar ratio of 5:1. These changes can be attributed to the small peak sizes and low signal-to-noise ratios, resulting in inaccurate crystallite size calculations. All experimental data for Figure 11 are summarized in Table S4 in the Supplementary Information.

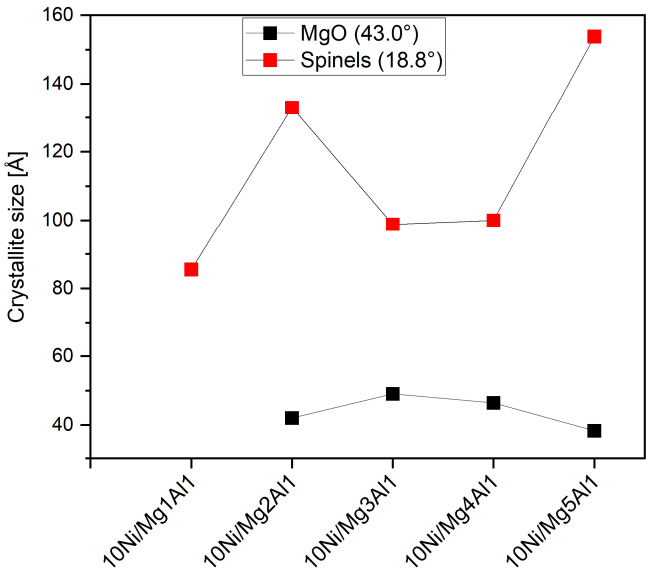

Figure 11. Crystallite sizes of the five Ni-containing catalysts prepared via the urea method.

2.2.3. Inductively Coupled Plasma with Optical Emission Spectroscopy (ICP-OES)

ICP-OES analyses were performed to verify whether the selected synthesis routes had resulted in the desired compositions of the individual catalysts. Table 5 summarizes the results. Regarding the Ni mass fractions, the table shows reasonable agreement between the measured values from the ICP-OES and the calculated values for the catalyst syntheses. Once again, the value for the 10Ni/Mg4Al1_urea catalyst was striking, as it is the only one that exceeds the calculated value of 10.96 wt% with 14.48 wt%. The smallest deviation between the measured and calculated values for the Ni mass fractions was found in the 10Ni/Mg5Al1_urea catalyst. In addition, a comparison of the measured and calculated values for the Mg/Al molar ratios revealed significant differences. For example, the measured Mg/Al molar ratio in the case of the 10Ni/Mg5Al1_urea catalyst was only approximately 1:1, although it should be around 5:1. This indicates that urea hydrolysis with the parameters described in Section 3.1.2 was insufficient to precipitate $Mg(OH)_2$ together with $Al(OH)_3$. This was because the highest pH value achieved during the 7.5 h reaction time was 8.5. However, the solubility product of $Mg(OH)_2$ indicates that a pH value of between 9 and 10 is required for sufficient precipitation, whereas $Al(OH)_3$ precipitates at a pH value of between 6 and 8. Therefore, $Mg(OH)_2$ could not completely precipitate in the urea hydrolysis, resulting in the low Mg/Al molar ratios in this table.

Table 5. Comparison of the Ni mass fraction and the molar ratios of Mg/Al (urea method) determined via (i) ICP–OES measurements and (ii) ciphered based on experimental quantities.

Catalysts	Ni Mass Fraction [wt%]		Mg/Al Molar Ratios [−]	
	ICP-OES	Calculated	ICP-OES	Calculated
10Ni/Mg1Al1_urea	8.96 ± 0.07	11.06	0.19:1	1.00:1
10Ni/Mg2Al1_urea	8.60 ± 0.11	11.00	0.33: 1	2.01:1
10Ni/Mg3Al1_urea	10.24 ± 0.16	11.35	0.68: 1	2.99:1
10Ni/Mg4Al1_urea	14.48 ± 0.04	10.95	0.84: 1	4.02:1
10Ni/Mg5Al1_urea	10.40 ± 0.30	10.96	1.06: 1	5.02:1

2.2.4. Scanning Electron Microscopy (SEM)

Figure 12 illustrates an SEM image of the Mg1Al1_urea support at a magnification of 2500 (top left), an SEM image of the catalyst Ni/Mg1Al1_urea at a magnification of 10,000 (top right), and EDX element mappings (bottom), which belong to the image at the top right.

The image of the Mg1Al1_urea support on the top left presents the surface of a larger structure on which some smaller particles were positioned. Thereby, even though their size differed, the small particles were evenly distributed. Furthermore, the image reveals irregularities on the surface of the larger structure. It can be assumed that the larger structure was made of an Al_2MgO_4 spinel formed during the precipitation process.

The image on the top right shows the surface of the larger structure in close detail. It reveals that the surface as well as the small particles were made of a layered framework, including pores and irregularities. From the EDX mappings, it can be derived that the small particles sticking to the surface of the mixed oxide consisted of the spinel structure Al_2MgO_4. A detailed size analysis reveals that the average size of the small particles was in the range of 1 μm^2 with a few particles exceeding 20 μm^2. EDX mapping for the Ni/Mg1Al1_urea catalyst shows that Ni was present on the surface of the catalyst support both as particles and as Al_2NiO_4 spinel.

2.2.5. N_2 Sorption

Table 6 shows the results of the N_2 sorption measurements for the five Ni-containing catalysts synthesized using the urea method and with the respective MgAl supports. Surface area values ranged from 167.9 $m^2\ g^{-1}$ for the 2:1 Mg/Al molar ratio to 288.2 $m^2\ g^{-1}$ for the 4:1 ratio, the latter being nearly twice as high. This means that there was no clear correlation between the specific surface area of the catalysts and their Mg/Al molar ratio. The same applied to the pore volumes: the 5:1 Mg/Al molar ratio had the smallest volume (0.24 $cm^3\ g^{-1}$), whereas the 1:1 ratio showed the largest (0.42 $cm^3\ g^{-1}$). Furthermore, the pore volumes were not linked to the specific surface areas, as the largest specific surface area belonged to the second lowest pore volume at the 4:1 Mg/Al molar ratio. A trend could be identified in the average pore size, where it decreased with increasing Mg/Al molar ratio, except for the 5:1 ratio, which had a larger average pore size than the 4:1 ratio. As no consistent trend emerged between the three properties derived from the N_2 sorption measurements and the Mg/Al molar ratios, it appears that the Mg/Al molar ratio did not crucially influence the surface or pores of the catalysts. When comparing the results for the surface area, the pore volume and the average pore size of the Ni-containing catalysts with their respective supports at the same Mg/Al molar ratio, it is noticeable that the undoped supports consistently exhibited higher numerical values. This trend was also observed for the catalysts from the co-precipitation route.

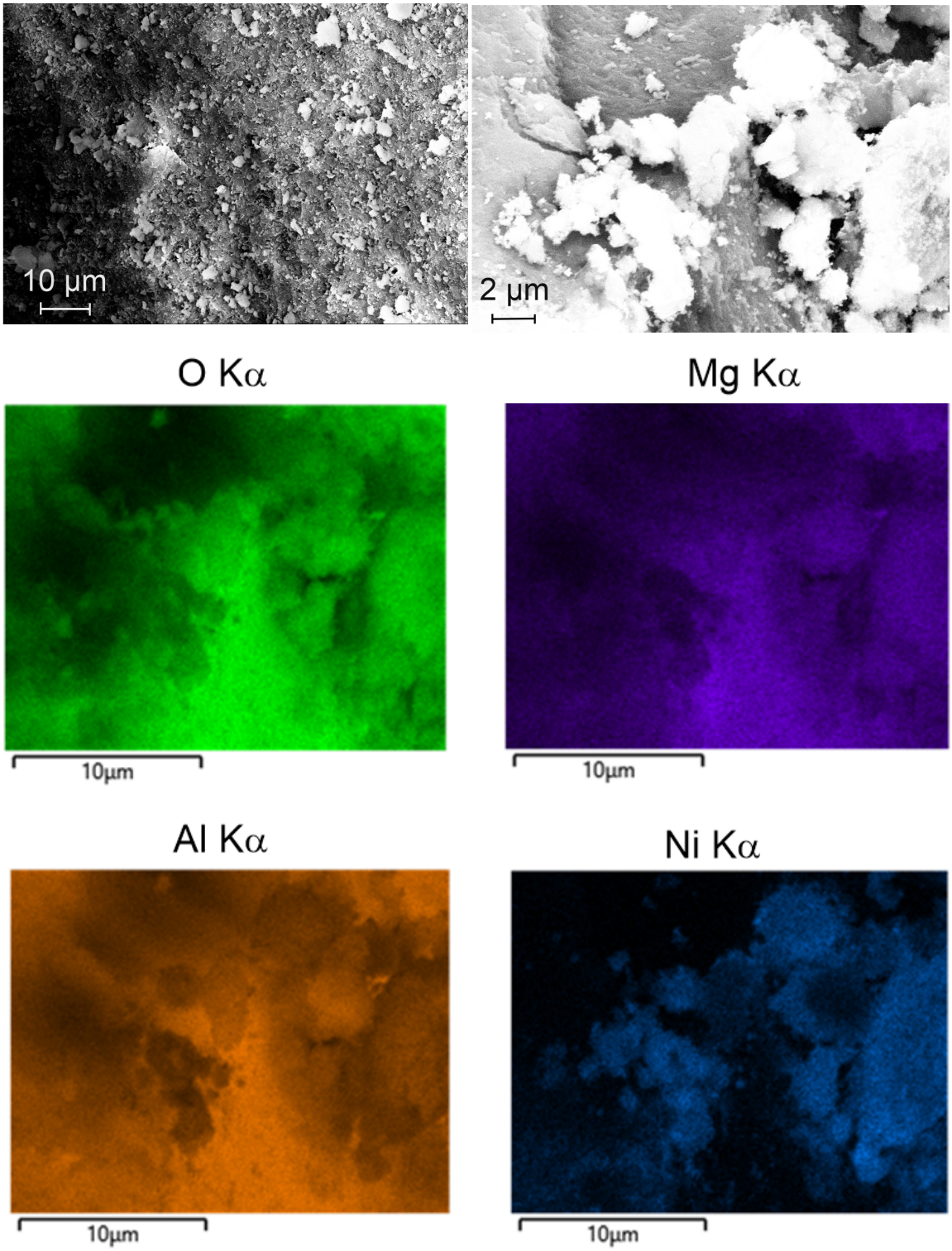

Figure 12. SEM image of the Mg1Al1_urea support at a magnification of 2500 (**top left**), SEM image of the catalyst Ni/Mg1Al1_urea at a magnification of 10,000 (**top right**), and EDX element mappings (**bottom**), which belong to the image at the top right.

Table 6. Results of the N_2 sorption measurements with the five catalysts synthesized via the urea method and with the respective supports.

Catalysts	Surface Area [m^2 g^{-1}]	Pore Volume [cm^3 g^{-1}]	Average Pore Size [Å]
Mg1Al1_urea	243.1	0.47	50.1
Mg2Al1_urea	204.0	0.38	42.7
Mg3Al1_urea	269.7	0.37	33.2
Mg4Al1_urea	303.4	0.32	25.4
Mg5Al1_urea	262.5	0.30	26.9
10Ni/Mg5Al1_urea	186.5	0.42	45.3
10Ni/Mg2Al1_urea	167.9	0.29	34.8
10Ni/Mg3Al1_urea	245.0	0.31	25.1
10Ni/Mg4Al1_urea	288.2	0.26	17.9
10Ni/Mg5Al1_urea	210.7	0.24	22.9

2.2.6. Catalytic Activity

Figure 13 depicts the results of the catalytic tests at a reaction temperature of 185 °C with the five catalysts prepared via the urea method. Blank experiments without catalyst but with all other components of the reactant mixture, including NaOH, showed no catalytic activity. For the representation of this figure, the actual values for the catalyst composition from Table 5 were chosen. The figure on the top left regarding the concentration of iso-butanol as a function of reaction time illustrates that with all catalysts, the concentrations of iso-butanol rose continuously up to a reaction time of 210 min. However, there was no clear dependence on the Mg/Al molar ratio of the respective catalysts. This is different from the case of co-precipitation catalysts, where a clear correlation was observed. While sample 10Ni/Mg0.68Al1_urea showed an iso-butanol concentration of 131 mmol L^{-1} at a reaction time of 210 min, the values of catalysts 10Ni/Mg0.33Al1_urea, 10Ni/Mg1.04Al1_urea, and 10Ni/Mg0.84Al1_urea were significantly higher and amounted to 161 mmol L^{-1}, 164 mmol L^{-1}, and 170 mmol L^{-1}, respectively, at this reaction time. These quantities are plainly higher than those of catalysts synthesized using the co-precipitation route with maximum values in the range of 140 mmol L^{-1} (see Figure 7). In comparison, Pasel et al. [29,30] and Häusler et al. [27,28] found significantly lower values for iso-butanol concentration in the range of 70 mmol L^{-1} to 80 mmol L^{-1} with their Pd/C, Pt/C, Ru/C, Ir/C, Rh/C, Cu/C, Ni/C and NiPt/C catalysts. At 150 °C, the Ni/C catalyst achieved an ethanol conversion of less than 1% with a selectivity for iso-butanol of 19%. The trends for all five catalysts in Figure 13 showed a slight decline after a reaction time of 240 min, suggesting the onset of deactivation. Since the selectivities towards iso-butanol of all five catalysts were similar, ranging between 85% and 90% (see part c of this figure), the dependencies described for the concentrations of iso-butanol can also be found in the conversion of ethanol. The maximum conversions were approximately 15%. From these descriptions, it can be concluded that within the series of catalysts from the urea method, no influence of the Mg/Al molar ratio on the catalytic activity can be deduced. It is possible that the values found via ICP-OES for the Mg/Al molar ratio between 0.19 and 1.06 were too similar to each other to cause a consistent effect among themselves. Explanations for the highest catalytic activity of sample 10Ni/Mg0.84Al1_urea among all ten samples from this paper may lie in its 100% proportions of strong basic and medium acidic catalyst centers and its large specific surface area of approximately 288 m^2 g^{-1}. In the lower section of Figure 13, the selectivities of the individual catalysts towards the products iso-butanol, 2-methylbutane-1-ol and 2,3-dimethylpentane-1-ol are plotted on the left *Y*-axis. The reaction time was 240 min. Selectivities towards 2,3-dimethylpentane-1-ol were in the range of 6–8%, while those towards 2-methylbutane-1-ol amounted to 4–8%. The space–time yield for the formation of

iso-butanol of the catalysts is shown in this figure on the right *Y*-axis at a reaction time of 240 min. It is highest for sample 10Ni/Mg0.84Al1 with a value of 8.0 mmol g^{-1} h^{-1}. The corresponding number at a reaction time of 210 min was 8.2 mmol g^{-1} h^{-1}. As with the case of the iso-butanol concentrations shown above, the figures for space–time yield were higher for the urea method than for the co-precipitation route. All experimental data for Figure 12 are summarized in Tables S5 and S6 in the Supplementary Information.

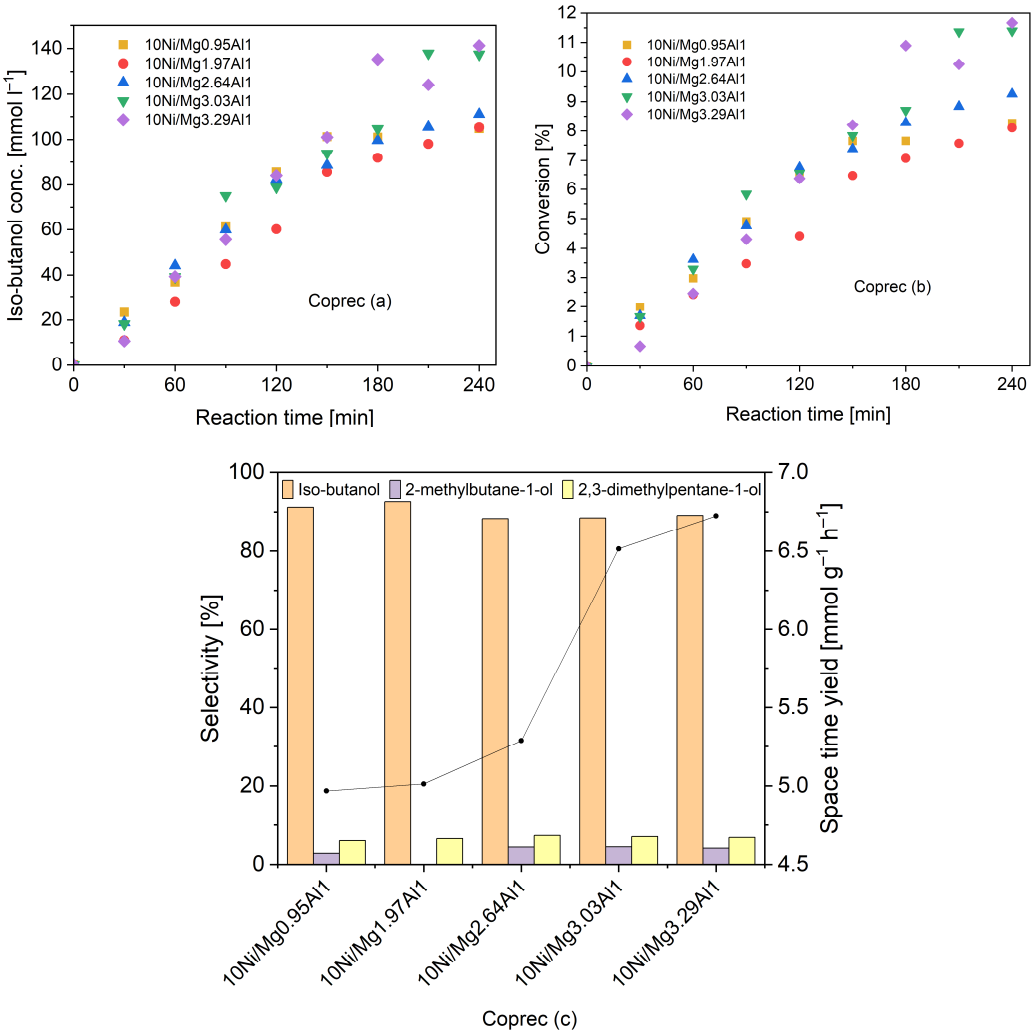

Figure 13. Results of the catalytic tests at a reaction temperature of 185 °C with respect to the synthesis of iso-butanol with the five catalysts prepared via the urea method, m(catalyst) = 250 mg, d(powder) < 75 µm, V(reactor) = 70 mL, c_0(EtOH) = 1600 mmol L^{-1}, c(NaOH) = 450 mmol L^{-1}, c(n-decane) = 15 mmol L^{-1}, methanolic solution. (**a**) Concentration of iso-butanol. (**b**) Ethanol conversion. (**c**) Selectivities towards iso-butanol and other main by-products (left), space–time yield at 240 min reaction time.

Table 7 compares the catalytic activity of the most promising catalyst from this paper, i.e., 10Ni/Mg0.84Al1_urea, with the catalytic behavior of other catalysts from the literature that were used under comparably mild reaction conditions for the synthesis of iso-butanol from mixtures of ethanol and methanol. It becomes clear that the Ni/MgO-Al_2O_3 catalyst from this paper exhibited outstanding values for ethanol conversion, iso-butanol concentration, selectivity to iso-butanol and space–time yield. These values constitute the uniqueness and innovation of the hydrotalcite-derived Ni/MgO-Al_2O_3 mixed oxides synthesized for this paper.

Table 7. Comparison of experimental results on the catalytic activity of the 10Ni/Mg0.84Al1_urea catalyst with data from the literature from other groups working under comparable conditions.

Catalysts/Reaction Conditions	Ethanol Conversion [%]	Iso-Butanol Concentration [mmol L^{-1}]	Selectivity to Iso-Butanol [%]	Space–Time Yield [%]	Reference
Ni/MgO-Al_2O_3, 185 °C, 6 bar N_2, 4 h	15.0	170	85–90	8.2	This work
$Ni_{99}Pt_1$/C, 180 °C, 6 bar N_2, 4 h	9.8	58	99	4.24	[29]
$Ni_{96}Pt_4$/C, 165 °C, 6 bar N_2, 4 h	12.7	74	95	4.72	[30]
Cu/Mg-Al, 200 °C, 100 h	11.0	-	70	-	[39]
Cu/Mg-Al, 200 °C, 12 h	40.0 *	-	-	-	[18]
Cu/Mg-Al, 210 °C	10.0	-	100	-	[23]

* calculated based on 1-propanol.

3. Materials and Methods

3.1. Synthesis of Hydrotalcite-Derived Mixed Oxide Supports

3.1.1. Synthesis via Co-Precipitation

The precipitation agent for the co-precipitation synthesis method was a solution containing 1 mol L^{-1} NaOH (Carl Roth GmbH & Co. KG, Karlsruhe, Germany) and 1 mol L^{-1} Na_2CO_3 (Thermo Fisher Scientific Inc., Waltham, MA, USA). To prepare the solution, 40 g of NaOH and 106 g of Na_2CO_3 were weighed in and dissolved in one liter of distilled water. The solution was stirred until all solids were dissolved in the distilled water.

To synthesize the different MgO-Al_2O_3 hydrotalcite supports, first, the respective calculated quantities of $Mg(NO_3)_2 \cdot 6\ H_2O$ and $Al(NO_3)_3 \cdot 9\ H_2O$ (Thermo Fisher Scientific Inc., Waltham, MA, USA) were weighed in. These quantities were fully dissolved in 200 mL of distilled water. The precipitation was conducted using an automatic titration unit (Metrohm 888 Titrando, Metrohm Deutschland GmbH & Co. KG, Filderstadt, Germany). With a speed of 2 mL min^{-1}, the precipitation agent was added to the nitrate precursor solution at room temperature, while the pH value was measured the entire time. Once the pH value had reached ten, the addition of the precipitation agent was stopped, and the suspension was stirred for 24 h at room temperature. The precipitate formed was then separated by removing the liquid phase in a Büchner funnel. To wash the separated precipitation, it was transferred into a beaker with 400 mL of distilled water. The suspension was then stirred (IKA RCT basic, IKA-Werke GmbH & Co. KG, Staufen, Germany) for 30min before the liquid phase was separated again in a Büchner funnel. This procedure was repeated until the pH value of the liquid phase, measured with a pH electrode (Metrohm 914 pH/Conductometer, Metrohm Deutschland GmbH & Co. KG, Filderstadt, Germany), reached seven. In the next step, the washed precipitation was dried at 100 °C for 2 hin a drying oven (homemade). Afterwards, it was calcined at 500 °C for 4 h in a chamber furnace (Carbolite CWF 12/13, Carbolite Gero Limited, Hope Valley, UK) to produce the oxidic forms and to remove the anion–water interlayer.

3.1.2. Synthesis via Urea Hydrolysis

To synthesize the different MgO-Al_2O_3 hydrotalcite supports via the urea hydrolysis method, again, the calculated quantities of $Mg(NO_3)_2 \cdot 6\ H_2O$ and $Al(NO_3)_3 \cdot 9\ H_2O$ were weighed in. These amounts were dissolved in 200 mL of distilled water together with a calculated amount of urea (Thermo Fisher Scientific Inc., Waltham, MA, USA). The quantity of urea was calculated to be 3.3 times the amount of the nitrates. This solution was then stirred until no solids were visible any more before transferring it quantitatively to a 500 mL three neck round bottom flask. To start the precipitation, the temperature of an oil bath (homemade) was set to 110 °C, while a magnet stirrer ensured the homogeneity of the solution. Once the solution temperature reached 90 °C, the precipitation time started. In

between, the pH value was monitored using pH indication paper and a pH electrode. The reaction was stopped after 7.5 h by removing the oil bath. Separating, washing and drying the precipitation as well as the calcination procedure were conducted the same way as in Section 3.1.1.

3.1.3. Wet Impregnation with Ni

Before the different MgO-Al_2O_3 hydrotalcite supports can be evaluated with respect to their catalytic activities, the active metallic Ni needs to be doped onto their surfaces. Therefore, $Ni(NO_3)_2 \cdot 6\ H_2O$ (Sigma-Aldrich, St. Louis, MO, USA) to achieve a Ni loading of 10 wt% on each of the respective supports was weighed in and dissolved in 50 mL of distilled water. To this Ni-ion-containing solution, 1.35 g of the synthesized supports from Sections 3.1.1 and 3.1.2, respectively, was added. Utilizing a rotary evaporator (IKA RV 8, IKA-Werke GmbH & Co. KG, Staufen, Germany) and a heating bath (IKA HB 10, IKA-Werke GmbH & Co. KG, Staufen, Germany), the suspension was dried. The evaporation of water was conducted with 60 rotations per minute (RPM) at a temperature of 60 °C and a pressure of 60 mbar. The dry catalyst was then calcined under the same conditions, as described in Section 3.1.1. To prepare for reduction, the precipitation was ground with a pestle and a mortar. Afterwards, the powder was reduced in a tube furnace (Heraeus ROK A 4/60, Heraeus Holding GmbH, Hanau, Germany) at 550 °C for 5 h with a flow of 2 vol% H_2 in N_2. Parmaliana et al. [40] report that NiO is reduced to elemental Ni in the temperature range between 250 °C and 550 °C, depending on the calcination temperature and Ni loading. MgO and Al_2O_3 show no reduction peaks up to a temperature of 1000 °C.

3.2. Catalytic Experiments

3.2.1. Test of Catalytic Behavior

The tests of catalytic behavior of the respective catalysts from the two synthesis routes were carried out in a batch reactor (model 4598, Inconell 600-alloy) from the company Parr (Parr instruments, Moline, IL, USA). The solutions for the reactions were prepared in a 100 mL volumetric flask. In each case, it contained 1.6 mol L^{-1} ethanol (Thermo Fisher Scientific Inc., Waltham, MA, USA), 0.45 mol L^{-1} NaOH and 0.015 mol L^{-1} n-decane (as internal standard, Sigma-Aldrich, St. Louis, MO, USA) in methanol (Merck KGaA, Darmstadt, Germany) as a solvent/reactant. First, 5 wt% catalyst, relative to the quantity of ethanol, was weighed and transferred to the reaction vessel. The atmosphere inside the reaction vessel was switched by the repeated passing in of N_2 up to a pressure of 6.0 bar. After the atmosphere in the vessel was replaced for the third time, 70 mL of the solution was filled into the vessel by injection through a membrane. Once the solution was inside the reaction vessel, the atmosphere was replaced by N_2 once more. Afterwards, the temperature inside the reactor was set to 185 °C, and the stirring speed was set to 1000 rotations per minute (rpm). Samples for gas-chromatographic and mass-spectrometric analysis (8890 GC and 5977B MSD from Agilent, Santa Clara, CA, USA) were taken from the reactor vessel every half an hour except for sample numbers 0, 1, 2 and 11. Sample 0 is a fraction of the remaining reaction solution not being filled into the vessel, while 1 is the first sample from the reaction vessel at room temperature before the reaction period starts. The second sample is taken once the solution reached 185 °C, and the eleventh sample is collected when the vessel was cooled down to room temperature again after the reaction period. The reaction lasted for 4 h, and the reaction time started for the second sample once the solution had reached 185 °C. For the gas-chromatographic measurements, 1 mL of solution is taken from the reaction vessel through a capillary after having flushed the capillary with 1 mL of the same solution.

3.2.2. Analysis via Gas-Chromatography and Mass Spectrometry (GC-MS)

For each GC-MS analysis, 3 µL of the respective collected sample was transferred to a 21 mL headspace vial using a 10 µL variable pipette (Eppendorf SE, Hamburg, Germany). The separation of the compounds took place in a GC, while the identification was conducted in an MS. The method used to analyze the samples was a full evaporation method to protect the column from undissolved NaOH or catalyst particles. For the full evaporation, the samples were preheated to a temperature of 105 °C for 5 min. An autosampler (PAL HTS-xt, Chromtech GmbH, Bad Camberg, Germany) was responsible for transporting and injecting the sample. After the evaporation, a gastight syringe (Hamilton Bonaduz AG, Bonaduz, Switzerland), V = 2.5 mL, syringe temperature = 100 °C, filling speed = 100 µL s^{-1}, flush time = 10 s, pull-up delay = 100 ms, injection speed = 500 µL s^{-1}, N_2 as flushing gas) took the samples and injected them into the back inlet of the GC. There, the samples were diluted with a 75:1 split with 99.9999% purity He as carrier gas. Afterwards, the sampled reached the column. It is a 30 m long DB-wax column with a diameter of 0.25 mm and a film thickness of 0.25 µm. The separation was conducted using the following temperature program for the column oven. For the first 4 min, the temperature stayed at 35 °C. Then, the temperature rose with a rate of 20 K min^{-1} until it reached 220 °C. This temperature was kept for 1 min before the analysis ended. The separated sample then flowed to the MS for structural identification. Due to electron impact ionization, the molecules in the samples break down into smaller fragments. These fragments are separated in a quadrupole because of their different mass–to–charge ratios (m/z). The electron multiplier with a high-energy dynode detects the fragments and allows the qualification of the compounds. To quantitate the reaction products, a calibration made from the pure substances is being applied, while n-decane is used as an internal standard.

3.3. Temperature-Programmed Methods

3.3.1. Temperature-Programmed Desorption of CO_2 (CO_2-TPD)

The procedure for sample preparation and installation in the Autochem III apparatus (Micromeritics GmbH, Unterschleißheim, Germany) was the same as described in Section 3.3.1 for TPR. Before CO_2 adsorption and subsequent desorption took place, the samples were pretreated. This means that all remaining adsorbed gases were eliminated by heating the samples with a rate of 50 k min^{-1} up to a temperature of 350 °C under a He flow of 50 mL min^{-1}. After cooling down back to room temperature, the adsorption of CO_2 started. Therefore, a flow of 50 mL min^{-1} CO_2 was fed through the sample for 1 h. Afterwards, 10 mL min^{-1} CO_2 flowed through the U-shaped glass with the samples for an additional 10 min. Once the adsorption steps were complete, the desorption was carried out. For that, the samples were heated with 3 k min^{-1} up to 700 °C. The TCD registered any change in the gas flow composition and thereby measured the amount of desorbing CO_2.

3.3.2. Temperature-Programmed Desorption of NH_3 (NH_3-TPD)

The procedure for sample preparation and their installation in the Autochem III apparatus were the same as described in Section 3.3.1 for TPR. The conditions of the experiments for NH_3-TPD were identical to those for CO_2-TPD with the exception that in this case, NH_3 was used instead of CO_2.

3.4. Structural Analysis

3.4.1. X-Ray Diffraction (XRD)

For the XRD measurement, a Bruker D8 DISCOVERY apparatus (Bruker Corporation, Billerica, MA, USA) with a LYNXEYE XE-T detector was used. The X-ray generator ran with 40.0 kV and 40.0 mA. About 50 mg of sample material was needed for the characterization.

It was irradiated with Cu-Kα-radiation with a wavelength of λ = 1.54060 Å. The 2θ angle was measured from 5° to 99.995° with a step length of 0.020°. Every step took 0.6 s. A Soller slit with an opening angle of 2.500° was applied for the primary ray path. For the analysis of the XRD spectra, the software DIFFRAC.EVA version 7.3 was used. With this software, the Scherer equation was applied to calculate the crystallite size for local peaks. Samples were calcined at 500 °C for four hours in N_2 and reduced at 550 °C for five hours in 2 vol% H_2 in N_2.

3.4.2. Inductively Coupled Plasma with Optical Emission Spectroscopy (ICP-OES)

The experimental procedure for conducting the ICP-OES analyses is described in detail by Häusler et al. and Pasel et al. [27,32].

3.4.3. Scanning Electron Microscopy (SEM)

The SEM images were recorded with a Zeiss Gemini Ultra Plus (Acceleration voltage = 20.00 kV; magnification from 250 to 10,000, Carl Zeiss AG, Oberkochen, Germany). The electrons were detected with an Oxford max 100 detector with a distance of 8.5 mm.

3.4.4. N_2 Sorption

The determination of the specific surface areas of the different hydrotalcite-derived samples was made following the explanation of Pasel et al. [12]. The Brunnauer–Emmett–Teller method was applied [41].

4. Conclusions

The uniqueness and innovation of the hydrotalcite-derived Ni/MgO-Al_2O_3 mixed oxides synthesized for this paper are demonstrated by the experimental findings that high concentrations of iso-butanol of up to 170 mmol L^{-1} with selectivities towards iso-butanol of 85–90% were achieved at a mild reaction temperature of 185 °C using a precious metal-free catalyst system. The key results of this paper are summarized below.

The CO_2-TPD profiles of the five samples from the co-precipitation method showed among themselves a very similar structure with predominantly strong basic sites. The NH_3-TPD profiles were also like each other with strong acidic centers dominating over weak acidic sites. In the case of the urea method, the 10Ni/Mg4Al1_urea sample stood out. It had 100% shares of strong basic and medium acidic sites.

In the X-ray diffraction patterns of the co-precipitated samples, reflections from NiO, MgO and the spinels Al_2NiO_4 and Al_2MgO_4 were detected. The experiments also showed that as the molar Mg/Al molar ratio increased, both the crystallinity and the crystallite sizes of MgO and the spinels increased. For the urea catalysts, the XRD showed characteristic reflections for NiO, MgO and the spinel phases Al_2NiO_4 and Al_2MgO_4, which was similar to the catalysts from the co-precipitation route. At a molar ratio of Mg/Al = 1:1, an additional reflection for metallic Ni occurred, indicating an incomplete reoxidation of the sample.

While the ICP-OES measurements indicated effective impregnation of the support with Ni for both preparation methods, the measured molar Mg/Al molar ratios showed clear differences from the calculations being more pronounced for the urea method. This indicates a reduced precipitation of $Mg(OH)_2$ in the presence of $Al(OH)_3$.

For the co-precipitated catalysts, higher molar Mg/Al molar ratios led to higher iso-butanol concentrations of around 140 mmol L^{-1}, while the selectivity towards iso-butanol ranged from 88% to 93% for all five catalysts. All catalysts from the urea route showed steadily increasing iso-butanol concentrations up to 210 min at 185 °C with no clear dependence on the molar Mg/Al molar ratio. The most active catalyst among all samples from this paper, i.e., 10Ni/Mg0.84Al1_urea, was characterized by 100% proportions of

strong basic and medium acidic catalyst sites and the largest specific surface area. It revealed an iso-butanol concentration of 170 mmol L^{-1} and an ethanol conversion of 15%. With the urea samples, selectivities to iso-butanol were similar compared with those of the co-precipitation samples (85–90%). The space–time yield at 210 min was highest for 10Ni/Mg0.84Al1 (8.2 mmol g^{-1} h^{-1}), again outperforming the co-precipitated samples.

Supplementary Materials: The following supporting information can be downloaded at https://www.mdpi.com/article/10.3390/catal16040357/s1, Table S1: Experimental data with respect to Figure 5, Table S2: Experimental data with respect to Figure 7a,b, Table S3: Experimental data with respect to Figure 7c, Table S4: Experimental data with respect to Figure 11, Table S5: Experimental data with respect to Figure 13a,b, Table S6: Experimental data with respect to Figure 13c.

Author Contributions: Conceptualization, Q.K.T.; Funding acquisition, R.P.; Investigation, J.H.; Methodology, Q.K.T.; Supervision, Q.K.T. and J.P.; Writing—original draft, J.P.; Writing—review and editing, J.P., Q.K.T., J.H. and R.P. All authors have read and agreed to the published version of the manuscript.

Funding: This paper was funded by the Deutsche Forschungsgemeinschaft (DFG, German Research Foundation)—491111487.

Data Availability Statement: The data supporting this article have been included as part of the Supplementary Information.

Acknowledgments: Special thanks are due to the fuel synthesis team at Jülich and all project and cooperation partners.

Conflicts of Interest: Joachim Pasel, Justus Hüging, Quoc Khanh Tran, and Ralf Peters are employed by the company Institute of Energy and Climate Research, IET-4: Electrochemical Process Engineering For-schungszen-trum Jülich GmbH, 52425 Jülich, Germany. The funding sponsors had no role in the design of the study; in the collection, analyses, or inter-pretation of data; in the writing of the manuscript; or in the decision to publish the results.

References

1. Liu, Q.; Xu, G.; Wang, X.; Mu, X. Selective upgrading of ethanol with methanol in water for the production of improved biofuel—Isobutanol. *Green Chem.* **2016**, *18*, 2811–2818. [CrossRef]
2. Gabriëls, D.; Hernández, W.Y.; Sels, B.; Van Der Voort, P.; Verberckmoes, A. Review of catalytic systems and thermodynamics for the Guerbet condensation reaction and challenges for biomass valorization. *Catal. Sci. Technol.* **2015**, *5*, 3876–3902. [CrossRef]
3. Li, X.; Li, X. Continuous upgrading of methanol and ethanol to isobutanol by heterogeneous catalysis over Cu-CeO_2/AC catalyst and the combination. *Mol. Catal.* **2024**, *569*, 114641. [CrossRef]
4. Peters, M.; Menne, A.; Gielisch, H. Synthesis of Sustainable Fuels and Intermediates from Ethanol and Methanol. *Chem. Ing. Tech.* **2022**, *94*, 1501–1508. [CrossRef]
5. Wingad, R.L.; Bergström, E.J.E.; Everett, M.; Pellow, K.J.; Wass, D.F. Catalytic conversion of methanol/ethanol to isobutanol—A highly selective route to an advanced biofuel. *Chem. Commun.* **2016**, *52*, 5202–5204. [CrossRef]
6. Yusoff, M.N.A.M.; Zulkifli, N.W.M.; Masjuki, H.H.; Harith, M.H.; Syahir, A.Z.; Khuong, L.S.; Zaharin, M.S.M.; Alabdulkarem, A. Comparative assessment of ethanol and isobutanol addition in gasoline on engine performance and exhaust emissions. *J. Clean. Prod.* **2018**, *190*, 483–495. [CrossRef]
7. He, D.; Zhou, J.; Fang, K. Upgrading of methanol and ethanol to higher alcohols over NixCe/Mg_2Al-LDO catalysts. *Mol. Catal.* **2025**, *580*, 115079. [CrossRef]
8. Kaperneka, V.; Maragoudaki, L.; Atsonios, K. Process analysis and techno-economic comparison of aviation biofuel production via microbial oil and ethanol upgrading. *Fuel* **2026**, *406*, 137118. [CrossRef]
9. Makoye, A.; Lónyi, F.; Solt, H.E.; Cannilla, C.; Bonura, G.; Novodárszki, G.; Barthos, R.; Valyon, J.; Nagy, T.; Vikár, A. Catalytic Upgrading of Ethanol to 1-Butanol Biofuel Additive Using Pd/MgO-Al_2O_3 and Bimetallic Pd-Cu/MgO-Al_2O_3 Mixed Oxide Catalysts. *Sustain. Chem.* **2025**, *6*, 44. [CrossRef]
10. Wang, J.; Li, W.-C.; Sun, D.-H.; He, L.; Zhou, B.-C.; Lu, A.-H. High-Selective Upgrading of Ethanol to C4–10 Alcohols over Hydroxyapatite Catalyst with Superior Basicity. *ACS Sustain. Chem. Eng.* **2025**, *13*, 36–45. [CrossRef]

11. Yuan, L.; Li, H.; Zhang, Z.; Fan, G.; Li, F. Highly Efficient Ethanol Upgrading to Higher Alcohols over Surface Acidity-Enhanced Cu-Based Catalysts. *Ind. Eng. Chem. Res.* **2025**, *64*, 4771–4783. [CrossRef]
12. Pasel, J.; Häusler, J.; Schmitt, D.; Valencia, H.; Meledina, M.; Mayer, J.; Peters, R. Ethanol Dehydrogenation: A Reaction Path Study by Means of Temporal Analysis of Products. *Catalysts* **2020**, *10*, 1151. [CrossRef]
13. Pizzoferrato, R.; Richetta, M. Layered Double Hydroxides (LDHs). *Crystals* **2020**, *10*, 1121. [CrossRef]
14. Trujillano, R.; Labajos, F.M.; Rives, V. Hydrotalcites, a rapid survey on the very recent synthesis and applications procedures. *Appl. Clay Sci.* **2023**, *238*, 106927. [CrossRef]
15. Bellotto, M.; Rebours, B.; Clause, O.; Lynch, J.; Bazin, D.; Elkaïm, E. Hydrotalcite Decomposition Mechanism: A Clue to the Structure and Reactivity of Spinel-like Mixed Oxides. *J. Phys. Chem.* **1996**, *100*, 8535–8542. [CrossRef]
16. Li, J.; Lin, L.; Tan, Y.; Wang, S.; Yang, W.; Chen, X.; Luo, W.; Ding, Y.-J. High Performing and Stable Cu/NiAlO$_x$ Catalysts for the Continuous Catalytic Conversion of Ethanol into Butanol. *ChemCatChem* **2022**, *14*, e202200539. [CrossRef]
17. Zhu, M.; Wang, Y.; Du, M.; Zhang, X.; Liu, H.; Qiao, Z.; Yang, J.; Peng, B.; Nie, L.; Li, Z. Cu-incorporated MgAl LDH Catalyst for Enhanced Bio-ethanol Upgrading to Butanol. *ChemCatChem* **2026**, *18*, e01437. [CrossRef]
18. Bravo-Suárez, J.J.; Subramaniam, B.; Chaudhari, R.V. Vapor-phase methanol and ethanol coupling reactions on CuMgAl mixed metal oxides. *Appl. Catal. A Gen.* **2013**, *455*, 234–246. [CrossRef]
19. Wu, Z.; Wang, P.; Wang, J.; Tan, T. Guerbet Reactions for Biofuel Production from ABE Fermentation Using Bifunctional Ni-MgO-Al_2O_3 Catalysts. *Catalysts* **2021**, *11*, 414. [CrossRef]
20. Cheng, F.-L.; Guo, H.-Q.; Cui, J.-L.; Hou, B.; Li, D.-B. Guerbet reaction of methanol and ethanol catalyzed by CuMgAlO$_x$ mixed oxides: Effect of M^{2+}/Al^{3+} ratio. *J. Fuel Chem. Technol.* **2018**, *46*, 1472–1481. [CrossRef]
21. Cheng, F.-L.; Guo, H.; Cui, J.; Hou, B.; Xi, H.; Jia, L.; Li, D. Coupling of methanol and ethanol over CuMgAlO$_x$ catalysts: The roles of copper species and alkalinity. *React. Kinet. Mech. Catal.* **2019**, *126*, 119–136. [CrossRef]
22. Carlini, C.; Flego, C.; Marchionna, M.; Noviello, M.; Galletti, A.M.R.; Sbrana, G.; Basile, F.; Vaccari, A. Guerbet condensation of methanol with n-propanol to isobutyl alcohol over heterogeneous copper chromite/Mg–Al mixed oxides catalysts. *J. Mol. Catal. A Chem.* **2004**, *220*, 215–220. [CrossRef]
23. Carlini, C.; Marchionna, M.; Noviello, M.; Galletti, A.M.R.; Sbrana, G.; Basile, F.; Vaccari, A. Guerbet condensation of methanol with n-propanol to isobutyl alcohol over heterogeneous bifunctional catalysts based on Mg–Al mixed oxides partially substituted by different metal components. *J. Mol. Catal. A Chem.* **2005**, *232*, 13–20. [CrossRef]
24. Larina, O.V.; Valihura, K.V.; Kyriienko, P.I.; Vlasenko, N.V.; Balakin, D.Y.; Khalakhan, I.; Čendak, T.; Soloviev, S.O.; Orlyk, S.M. Successive vapour phase Guerbet condensation of ethanol and 1-butanol over Mg-Al oxide catalysts in a flow reactor. *Appl. Catal. A Gen.* **2019**, *588*, 117265. [CrossRef]
25. Tang, X.; Song, C.; Li, H.; Liu, W.; Hu, X.; Chen, Q.; Lu, H.; Yao, S.; Li, X.-N.; Lin, L. Thermally stable Ni foam-supported inverse CeAlO$_x$/Ni ensemble as an active structured catalyst for CO_2 hydrogenation to methane. *Nat. Commun.* **2024**, *15*, 3115. [CrossRef]
26. Chen, X.; Zhang, Y.; Sun, C.; Wang, Y.; Song, G.; Li, C.; Lim, K.H.; Ye, R.; Peng, Y.; Arandiyan, H.; et al. Lanthanum-mediated enhancement of nickel nanoparticles for efficient CO_2 methanation. *Fuel* **2024**, *371*, 131998. [CrossRef]
27. Häusler, J.; Pasel, J.; Wöllhaf, C.; Peters, R.; Stolten, D. Dilute Alloy Catalysts for the Synthesis of Isobutanol via the Guerbet Route: A Comprehensive Study. *Catalysts* **2024**, *14*, 215. [CrossRef]
28. Häusler, J.; Pasel, J.; Woltmann, F.; Everwand, A.; Meledina, M.; Valencia, H.; Lipińska-Chwałek, M.; Mayer, J.; Peters, R. Elucidating the Influence of the d-Band Center on the Synthesis of Isobutanol. *Catalysts* **2021**, *11*, 406. [CrossRef]
29. Pasel, J.; Häusler, J.; Peters, R.; Stolten, D. Catalytic activity and stability of NiPt/C catalysts for the synthesis of iso-butanol from methanol/ethanol mixtures. *Catal. Sci. Technol.* **2024**, *14*, 7048–7060. [CrossRef]
30. Pasel, J.; Häusler, J.; Peters, R.; Stolten, D. NiPt catalysts for the synthesis of iso-butanol: The influence of molar ratio and total metal loading on activity and stability. *Catal. Sci. Technol.* **2025**, *15*, 2248–2260. [CrossRef]
31. Pasel, J.; Häusler, J.; Schmitt, D.; Valencia, H.; Mayer, J.; Peters, R. Aldol condensation of acetaldehyde for butanol synthesis: A temporal analysis of products study. *Appl. Catal. B Environ.* **2023**, *324*, 122286. [CrossRef]
32. Pasel, J.; Woltmann, F.; Häusler, J.; Peters, R. Surface Redox Reaction for the Synthesis of NiPt Catalysts for the Upgrading of Renewable Ethanol/Methanol Mixtures. *Catalysts* **2024**, *14*, 77. [CrossRef]
33. Othman, M.; Helwani, Z.; Martunus; Fernando, W. Synthetic hydrotalcites from different routes and their application as catalysts and gas adsorbents: A review. *Appl. Organomet. Chem.* **2009**, *23*, 335–346. [CrossRef]
34. Costantino, U.; Marmottini, F.; Nocchetti, M.; Vivani, R. New Synthetic Routes to Hydrotalcite-Like Compounds − Characterisation and Properties of the Obtained Materials. *Eur. J. Inorg. Chem.* **1998**, *1998*, 1439–1446. [CrossRef]
35. Tran, Q.K.; Hüging, J.; Pasel, J.; Peters, R. Iso-Butanol Production as a Sustainable Chemical from Renewable Methanol/Ethanol Upgrading Using Ni/Cu-Al Hydrotalcite-Derived Catalysts Under Mild Conditions. *Chem. Eng. J. Adv.* **2026**, *26*, 101150. [CrossRef]
36. Choudhary, V.R.; Rane, V.H. Acidity/basicity of rare-earth oxides and their catalytic activity in oxidative coupling of methane to C2-hydrocarbons. *J. Catal.* **1991**, *130*, 411–422. [CrossRef]

37. Bartholomew, C.H.; Farrauto, R.J. Catalyst Characterization and Selection. In *Fundamentals of Industrial Catalytic Processes*; Wiley: Hoboken, NJ, USA, 2005; pp. 118–196.
38. Gražulis, S.; Daškevič, A.; Merkys, A.; Chateigner, D.; Lutterotti, L.; Quirós, M.; Serebryanaya, N.R.; Moeck, P.; Downs, R.T.; Le Bail, A. Crystallography Open Database (COD): An open-access collection of crystal structures and platform for world-wide collaboration. *Nucleic Acids Res.* **2012**, *40*, D420–D427. [CrossRef]
39. Marcu, I.-C.; Tichit, D.; Fajula, F.; Tanchoux, N. Catalytic valorization of bioethanol over Cu-Mg-Al mixed oxide catalysts. *Catal. Today* **2009**, *147*, 231–238. [CrossRef]
40. Parmaliana, A.; Arena, F.; Frusteri, F.; Giordano, N. Temperature-programmed reduction study of NiO–MgO interactions in magnesia-supported Ni catalysts and NiO–MgO physical mixture. *J. Chem. Soc. Faraday Trans.* **1990**, *86*, 2663–2669. [CrossRef]
41. Brunauer, S.; Emmett, P.H.; Teller, E. Adsorption of Gases in Multimolecular Layers. *J. Am. Chem. Soc.* **1938**, *60*, 309–319. [CrossRef]

Disclaimer/Publisher's Note: The statements, opinions and data contained in all publications are solely those of the individual author(s) and contributor(s) and not of MDPI and/or the editor(s). MDPI and/or the editor(s) disclaim responsibility for any injury to people or property resulting from any ideas, methods, instructions or products referred to in the content.